SENSITIVITY OF SIMULATED HURRICANE EYEWALL REPLACEMENT CYCLES TO HORIZONTAL TURBULENT MIXING

JOANNE MICHELLE KENNELL

A THESIS SUBMITTED TO
THE FACULTY OF GRADUATE STUDIES
IN PARTIAL FULFILLMENT OF THE REQUIREMENTS
FOR THE DEGREE OF
MASTER OF SCIENCE

GRADUATE PROGRAM IN
EARTH, SPACE AND ATMOSPHERIC SCIENCES
YORK UNIVERSITY
TORONTO, ONTARIO

AUGUST 2016

Acknowledgements

I would like to thank my thesis advisor Professor Yongsheng Chen for his support and motivation during my Masters research and coursework. His extreme patience, knowledge, and motivation helped me a great deal during times where I felt overwhelmed. He continuously believed in my capabilities and I am forever grateful.

I would also like to thank my thesis committee member Professor Gary Klaassen for his kindness and support.

Additionally, I would like to thank my friends and family who have supported me through the years of completing my graduate degree: Janice Kennell, Ernest Kennell, Laura Kennell-Morrison, Shannon Correia, Heather Ochoa, Navita Singh, Carolyn Rennie, Richard Liang, Sopan Kurkute, and most especially Mark Kunkel. Without his love and support this thesis would not be possible. He is my rock.

Abstract

Eyewall replacement cycles (ERCs) are naturally occurring phenomena in some intense tropical cyclones. The exact mechanisms of ERCs are currently not known and successful numerical simulations of ERCs are also very rare. The objectives of this thesis are to 1) validate the current ERC theories for a set of numerical simulations which resolved ERC processes, 2) investigate the role of boundary layer turbulence in ERCs, and 3) propose a mechanism for ERCs. Using the Advanced Research and Weather Forecasting (WRF-ARW) model, Hurricane Danielle (2010) was simulated. The ERCs that occurred in simulated Danielle are sensitive to parameterized horizontal turbulent mixing. Five theories on the initiating mechanisms of eyewall replace cycles are discussed with respect to each of our simulations and based on the results, a new idea of how the eyewall replacement process formed in our simulations is proposed. Two sensitivity experiments are performed to test the validity of this mechanism.

Table of Contents

List of Figures

List of Tables

Chapter 1: Introduction

Hurricanes are one of the most powerful natural hazards capable of inflicting a lot of damage and they impact millions of people every year. Hurricanes are known for very strong winds, storm surges, and tremendous amounts of rainfall that can result in coastal flooding, and the cost to fix the damages incurred can soar as high as hundreds of billions of dollars. Improvements to the forecasting of hurricane intensity, dynamics, structure, and rapid intensity change are a necessary part of the solution to reduce the number of hurricane-related fatalities and damage impacts.

1.1 Hurricane Dynamics

Hurricanes are synoptic-scale low pressure, warm-core systems that develop over the tropical oceans in regions with warm surface water temperatures (26.5 degrees Celsius or higher). They receive their energy from warm, moist air above warm and sufficiently deep (at least 50 metres) surface water. Air being converged and spiralled counter-clockwise towards the hurricanes low-pressure centre travels over this warm ocean water, leading to evaporation of the ocean surface water. This converging air loses angular momentum to the ocean, but gains heat stored as water vapour, resulting in very high moisture levels in the air entering the hurricane. As the air rises around the eye and rainbands of the hurricane, water vapour in the air condenses and latent heat is released to maintain the buoyancy needed for ascent. These updrafts in the eyewall entrain (draw) additional moist, midlevel (2-6 km) air, which results in a horizontal convergence of air toward the hurricane centre. This convergence supplies mass and angular momentum needed to spin-up the hurricane. In response to this latent heat release (warming) and decrease in air density, the pressure at the surface falls. Lower pressure at the surface results in even more moist air entering the hurricane. This process starts a chain reaction and is the driving “fuel” source for a hurricane.

Hurricanes rotate counter-clockwise due to the Coriolis force. The Coriolis force is

a natural phenomenon that causes a deflection to the right of fluids, such as the air, in the Northern Hemisphere, and it is important for hurricane formation. Hurricanes need the Coriolis force for rotation to begin. In fact, hurricanes cannot develop at or near the equator (between 5^{o} north and 5^{o} south) because the Coriolis force is non-existent or too weak.

A hurricane consists of two dominant circulations as well as asymmetries: the primary circulation (horizontal axisymmetric) (Figure 1), the secondary circulation (radial and vertical) (Figure 2), and wavenumber-1 asymmetries (*Marks,* 2003). Four forces produce the primary circulation of a hurricane: the pressure gradient force, the Coriolis force, the centrifugal force, and friction. The pressure gradient force always moves air from areas of high pressure to areas of low pressure. Since the lowest pressure of a hurricane is found at its centre, the pressure gradient force is always directed toward the centre (or eye) of a hurricane. The Coriolis force, as mentioned earlier, deflects air to the right in the Northern Hemisphere, and a faster rotating hurricane results in a stronger Coriolis force. The centrifugal force always acts outward from a rotating object and is also larger when the hurricane rotation is faster. The balance between the pressure gradient, Coriolis, and centrifugal force is called gradient wind balance. Upper level winds are in gradient wind balance since there is no frictional drag high in the atmosphere. However, friction causes air near the surface to move slower which reduces the Coriolis and centrifugal forces. But this friction does not affect the strength of the pressure gradient. Friction results in an imbalance of forces near the surface and therefore the near-surface wind is turned inwards towards the eye, resulting in air rotating inward and counter-clockwise towards the hurricane centre.

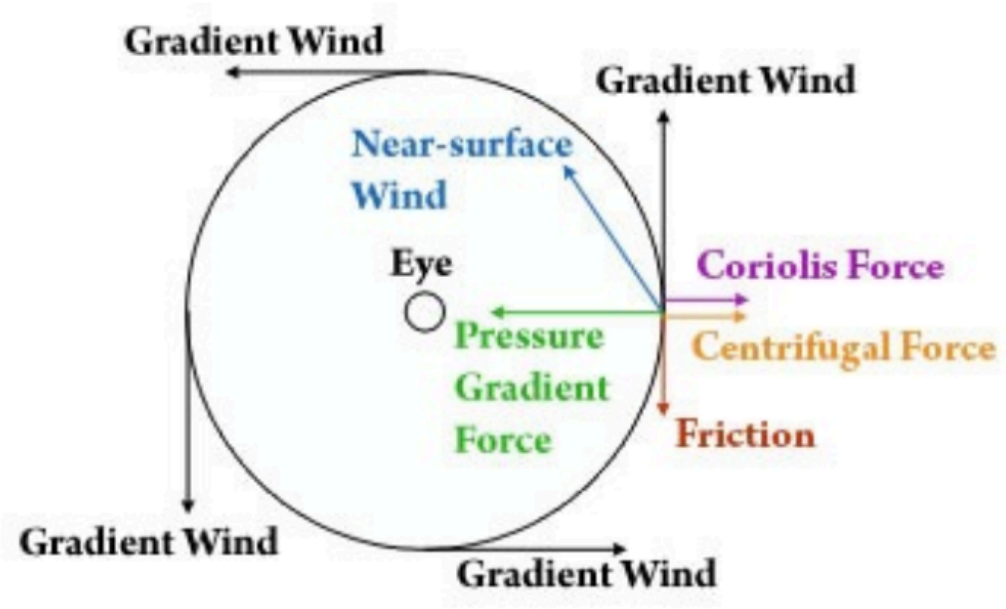

Figure 1: A simple schematic showing the primary circulation force balance (*Knowlton, 2015*)

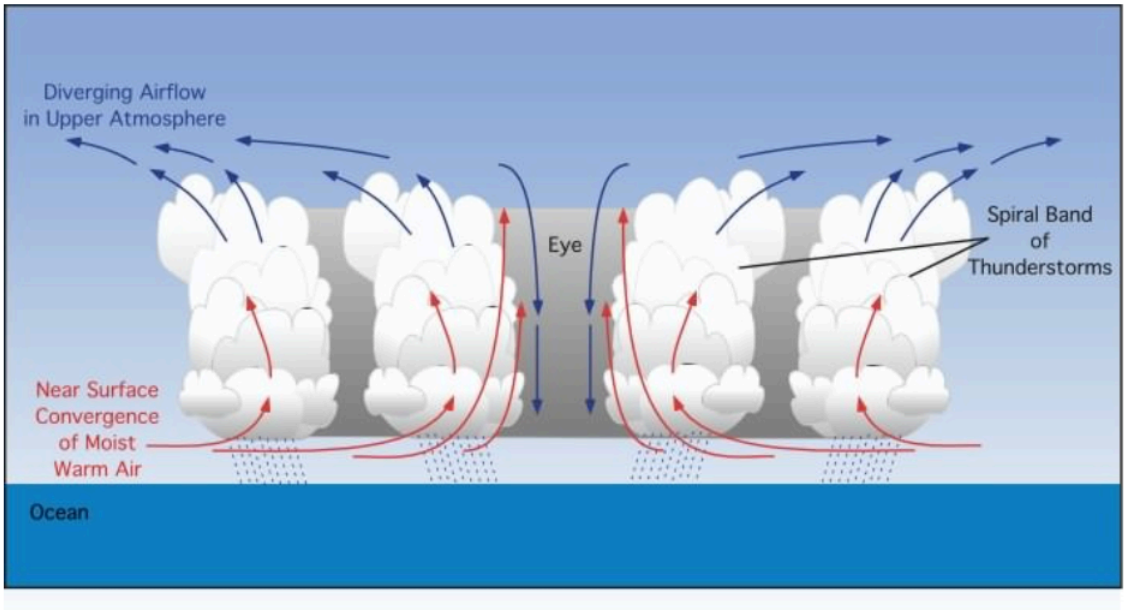

Figure 2: Secondary circulation of a hurricane (*Pidwirny, 2012*)

The warm-core of a hurricane (Figure 3) produces an expanded troposphere (lowest layer of the atmosphere) in the vertical (gets wider with increasing height). This creates a pressure gradient at the top of the hurricane that is much weaker than the pressure gradient close to the surface. This results in cyclonically (counter-clockwise) air flowing

into the hurricane near the surface while air exiting the hurricane at upper levels rotates anticyclonically (clock-wise). If the upper level winds remain weak, a balance between the convergence at the surface and divergence aloft will continue to fuel the hurricane.

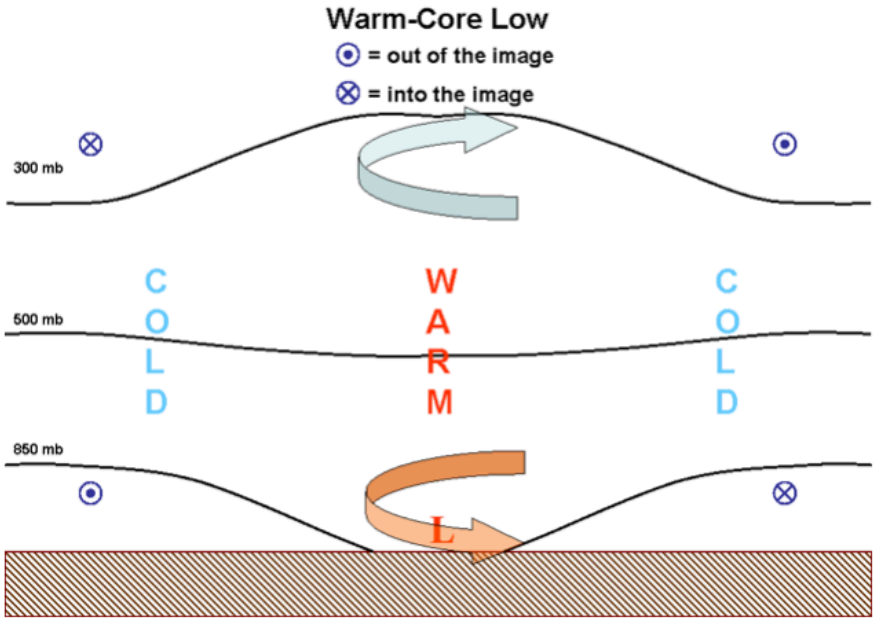

Figure 3: Schematic of a warm-core low-pressure system (*Simpson, 2012*)

Superimposed on the primary circulation is a weaker, forced secondary (*see* Figure 2) symmetric circulation (*Chan and Kepert, 2010*). The secondary circulation consists of frictional inflow in the boundary layer that loses angular momentum to the ocean, but gains heat in the form of warm and moist water vapour — resulting in very high moisture levels of air entering the hurricane, up-flow in the eyewall and rainbands that brings latent heat to upper levels through condensation, and outflow beneath the tropopause (layer between the troposphere and stratosphere). The secondary circulation is mainly produced by surface friction and latent heat release, and it redistributes heat and angular momentum, sustaining the primary circulation.

Wavenumber-1 asymmetries within the hurricane circulation, which are characterized as cyclonic and anticyclonic vortices centred on the radius of maximum wind (*Marks,* 2003), are caused by the storm's motion and shear of the mean horizontal

wind, both of which are related to environmental flow. An increase in wind shear results in the development of wavenumber-1 asymmetries, which are important at and inside the hurricane's radius of maximum wind (the distance between the hurricane's centre and its eyewall).

1.2 Hurricane Structure

A hurricane is composed of three main parts: the eye, the eyewall, and the outer rainbands.

1.2.1 The Eye

The eye of a hurricane is a usually cloudless region in the centre of a hurricane around which the entire storm rotates. The eye is relatively calm with light winds, has the lowest surface pressure (up to 10 percent less than surrounding regions), and its diameter can range from 5-200 km (*Chan et al., 2014*). Air parcels within the eye descend. This descent suppresses the development of clouds and precipitation, resulting in the relatively cloud and precipitation free region. This subsidence also results in compressional warming, causing the temperature in the eye to increase at the surface and aloft. The temperature aloft can be up to 10°C warmer while only 0-2°C warmer at the surface (*Hawkins and Rubsam, 1968*).

The size of the eye does not have a consistent width from the surface to the top of the hurricane. The eye width grows larger with height. This is due to a lack of friction in the upper levels and a weakening pressure gradient. As friction decreases, the wind speed increases and since the Coriolis and centrifugal forces are directly proportional to the wind speed, they increase as well. On the other hand, the pressure gradient force decreases. This change in force imbalance results in air parcels higher in the atmosphere to rotate around the eye at a larger radius and at a slower speed. At the top of the hurricane, the winds actually begin to rotate anticyclonically.

1.2.2 The Eyewall

The eye of a hurricane is surrounded by a ring of convective cloud, known as the eyewall, which rises and slopes radially outward from just above the ocean surface to the tropopause. The size of the eyewall can range from 8-50 km wide (*Chan et al., 2014*), and the strongest winds and heaviest rains of a hurricane are also found there. As air parcels move toward the centre of the hurricane, the distance between the air parcels and the centre of rotation decreases. Since air parcels must maintain their angular momentum due to the conservation of angular momentum, the speed of the air parcels must increase as they approach the hurricane centre. The convergence of air parcels is strongest at the eyewall compared to any other region of the hurricane, resulting in maximized latent heat release, convection, and heavy precipitation.

1.2.3 The Outer Rainbands

The outer rainbands are rings of convective clouds that spiral slowly counter-clockwise towards the eye and around the eyewall from the outer region of the storm. The rainbands generate most of the precipitation associated with a hurricane, and have also been known to produce tornadoes. The size of the rainbands can range from 4-40 km in width and 80-500 km in length (*Thornton, 2006*). In between the rainbands, subsidence of air parcels occurs. This results in compressional warming and a relatively rain-free region between rainbands. This warming between rainbands may contribute to an even lower surface pressure, which may result in the overall intensification of the hurricane. The relationship between the outer rainbands and the eye in intensifying a hurricane is not completely understood and is an area of current research.

1.3 Hurricane Boundary Layer

The hurricane boundary layer is defined as a shallow layer, typically 500 metres to 1 kilometre, of strong radial inflow close to the sea-surface and it is formed, in part,

because of the disruption of gradient wind balance due to friction near the surface. Hurricanes interact with the ocean through the boundary layer by obtaining heat and moisture, and transferring momentum to the oceans in the form of waves and currents (*Zhang, 2010*). The hurricane boundary layer is an important storm feature because it impedes the radial transport of vertical motion, absolute angular momentum, and moisture at the top of the boundary layer. It is believed that the hurricane boundary layer also plays an important role in the intensification process of a hurricane. Unfortunately, it is the least well understood part of a hurricane, as it is very dangerous to fly aircraft that low into the hurricane to gain in-situ data.

Turbulent mixing is the primary mechanism for the vertical transport of energy, moisture, and momentum in the hurricane boundary layer. Improved knowledge of the underlying mechanisms of exchanges between the boundary layer and the ocean is important since these processes currently need to be parameterized in numerical models (*Bryan et al., 2009*). In a study conducted by *Rotunno et al., (2012*), horizontal diffusion was found to be the most important control factor for the maximum simulated hurricane intensity. They showed that horizontal diffusion was a major contributor to the angular momentum budget in the boundary layer of the simulated storms. A better understanding of the physical and dynamical processes that occur in the hurricane boundary layer will lead to improve hurricane forecasting.

1.4 Eyewall Replacement Cycles

Eyewall replacement cycles (ERCs) are naturally occurring phenomena in some intense tropical cyclones that are generally Category 3 or higher on the Saffir-Simpson scale (*Chan and Kepert, 2012*). Although the exact mechanism(s) and dynamics that initiate the formation of an eyewall replacement cycle are currently not known, and are the topic of this thesis, the steps involved in the replacement process once the outer eyewall has formed are well documented.

Initially, the outer spiral rainbands organize into a distinct ring of thunderstorms, or

secondary eyewall, at a greater radius from the storm centre than the current eyewall. The region between the inner and outer eyewall is called the moat. The processes in the moat are currently not well understood, but the moat has been shown to be dynamically similar to the hurricane eye (*Houze et al., 2007*) and is believed to assist in the decay of the inner eyewall during the replacement process by producing subsidence over the inner eyewall. This subsidence is believed to suppress convection and weaken the inner wind maximum by increasing surface divergence (*Chan and Kepert, 2012*).

Once the secondary eyewall has formed, it intensifies and may begin to slowly contract inwards. The outer eyewall consumes high enthalpy air from the boundary layer inflow, robbing the inner eyewall of environmental moisture and angular momentum. The outer eyewall also weakens the inner eyewall by producing subsidence over the inner eyewall. During this replacement process, the intensity of the hurricane is weakening because the maximum winds are decreasing and the central pressure is rising as the inner eyewall is destroyed. Eventually the outer eyewall replaces the inner eyewall completely — timing can range from a few hours to more than a day (*Zhou and Wang, 2011*). The new eyewall may remain the same size or contract in radius, intensifying the storm to the same strength, or sometimes an even stronger hurricane, if in a favourable environment. This process may repeat several times during a hurricanes lifecycle (*Chan and Kepert, 2012*).

1.5 Observed Eyewall Replacement Cycles

Eyewall replacement cycles are known to cause rapid intensity and structure changes, including changes in wind speed and precipitation. These rapid changes may lead to stronger storm surges and an increase in coastal destruction as the secondary eyewall forms and begins to re-intensify at a larger radius than the initial eyewall. Examples of such changes occurred in Hurricane Ivan (2004) and Hurricane Rita (2005).

Hurricane Ivan reached a peak intensity of 140 knots — Category 5 — with an eye diameter of 35 km on September 8, 2004. Ivan weakened to a Category 4 hurricane due

to an eyewall replacement cycle, and re-intensified back into a Category 5 hurricane with a peak intensity of 145 knots on September 11th. Ivan once again weakened to a Category 3 hurricane due to a second eyewall replacement cycle on September 14th (*Stewart, 2004*). This resulted in a slow weakening and increase in eye diameter to 75-90 km as it made landfall west of Gulf Shores, Alabama. This enlargement of the eye, although a weaker hurricane, lead to widespread damage extending to the southern Alabama-western Florida panhandle border (Figure 4).

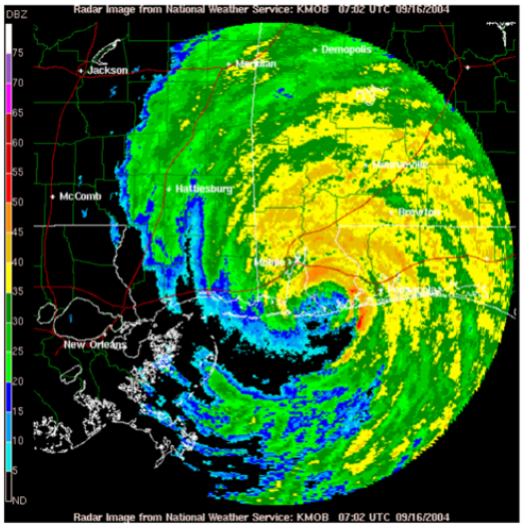

Figure 4: Reflectivity of Hurricane Ivan on September 16, 2004 after it already underwent an ERC and has moved onto land (*Stewart, 2004*)

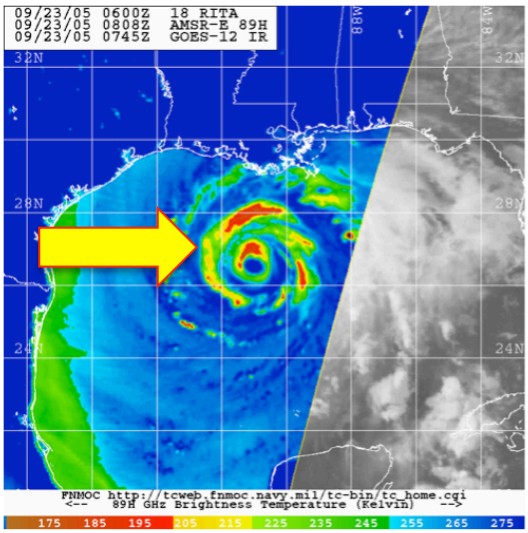

Figure 5: Reflectivity of Hurricane Rita on September 23, 2005 just before making landfall (*Knabb et al., 2006*)

Hurricane Rita developed into a Category 5 hurricane (145 knots) on September 21, 2005 with an eye diameter of approximately 35 km. On this date, Rita also weakened to a Category 4 hurricane due to an eyewall replacement cycle (*see* Figure 5). Rita continued to weaken to a Category 3 hurricane (110 knots) before making landfall (*Knabb et al., 2006*). Due to the weakening caused by the ERC, Rita's eye diameter increased to 55 km and hurricane force winds extended 250 km inland. Hurricane Rita resulted in large evacuations and significant storm surges in southwest Louisiana.

The initiating mechanisms that begin an eyewall replacement cycle are not well understood. Early observational studies of this process were limited by a lack of observations in the inner core and rainband regions (*Ortt, 2006*). The Hurricane Rainband and Intensity Experiment (RAINEX) performed in 2005 was designed to address this lack of observations. During RAINEX, aircraft missions collected airborne dropsonde data from Hurricane Katrina and Hurricane Rita (*Houze et al., 2005*). These storms were both major Category 5 hurricanes, but Katrina maintained one primary eyewall with no ERC while Rita developed a secondary eyewall and subsequent ERC. The observations gathered in this project have been compared with high-resolution model simulations in many papers attempting to solve the initiating ERC mechanism mystery.

1.6 Thesis Objectives

Rapid intensity change is a challenging task for operational hurricane forecasting. Studying the dynamics of eyewall replacement cycles can improve our understanding and ability to forecast such rapid intensity and structure changes of hurricanes, as well as assessing the impacts of hurricanes, which include human, economical, and environmental.

In recent modeling studies, it was found that the ERC in simulated hurricanes is sensitive to parameterized horizontal diffusion (*Chen and Kurkutes, 2012*). The main objective of this thesis is to investigate the effect of changes in the parameterized horizontal turbulent mixing length on a hurricane's eyewall replacement process using

the Advanced Research WRF (WRF-ARW) model. The sensitivity of horizontal turbulent mixing is tested by varying the Smagorinsky constant C_s, which is related to the horizontal mixing length l_h, of real case study Hurricane Danielle (2010). The properties and characteristics of the simulated ERCs will be diagnosed and compared to relevant papers and the real case of Hurricane Danielle (2010). The objectives of this thesis are as follows:

- Validate the current eyewall replacement cycle theories.
- Investigate the role of boundary layer turbulence in eyewall replacement cycles.
- Propose a hypothesis for an eyewall replacement cycle initiating mechanism.

Chapter 2: Literature Review

Eyewall replacement cycles were first documented as early as the 1950's (*Fortner, 1958*). Despite the amount of research that has been conducted to understand the initiating mechanism(s) of ERCs, there are still competing theories. There have been many different external and internal forcing mechanisms proposed over the years. It is now widely accepted by the scientific community that internal dynamics and favourable external environmental conditions are essential for ERC (*Sun, 2013*).

A review of several hypothesized mechanisms of eyewall replacement cycles are presented.

2.1 Formation of the Secondary Eyewall

2.1.1 External Mechanisms

Many external forcing mechanisms have been proposed for secondary eyewall formation. For example, *Willoughby* (1979) hypothesized that the secondary eyewall was formed by asymmetric friction due to the storm's motion. Many model simulations performed since then did not include systematic storm motion, but the simulated hurricane still developed a secondary eyewall. This suggests that this mechanism is not able to explain the formation of a secondary eyewall in simulations without this motion. *Hawkins* (1983) proposed that secondary eyewalls are formed by topographic forcings. Model simulations from several studies that formed a secondary eyewall did not include topographic forcings. This suggests that although topographic forcings is a possible reason for secondary eyewalls to form over topography, it is unable to explain the formation of a secondary eyewall in the absence of topography. *Molinari and Vollaro* (1990) and *Nong and Emanuel* (2003) proposed that synoptic-scale forcings lead to an eyewall replacement. This mechanism is unfortunately not able to explain the formation of a secondary eyewall in model simulations that do not include synoptic-scale forcings.

Favourable external environmental conditions for secondary eyewall formation include high convective available potential (CAPE), moisture distribution, and vertical wind shear (*Sun, 2013*). These external conditions affect the intensity and structure of a hurricane. High CAPE (the amount of energy that is available for an air parcel to undergo convection) is important for the formation of deep convection in the secondary eyewall formation region. It was noted by *Judt and Chen* (2010) that the moisture distribution of hurricanes might be important in the formation of a secondary eyewall. This topic is an area of current research and is discussed in this thesis. Moderate vertical wind shear (6 to 10 s^{-1}) was found, using a 3-D regional model with all model physics deactivated and a hurricane-like vortex in the presence of west-east vertical wind shear, to inhibit the formation of a secondary eyewall (*Menelaou et al., 2014*). In fact, a secondary eyewall only formed in the presence of weak vertical wind shear. However, this result still has to be addressed using a 3-D full physics model. The conditions listed above are areas of current research in terms of how and why they are important for secondary eyewall formation.

2.1.2 Internal Mechanisms

Theories of ERC formation are summarized and grouped below into categories based on the initiating mechanisms:

2.1.2.1 *Axisymmetrization with a Beta-Skirt*

Many mature hurricanes have a "skirt" of vertical vorticity outside of the primary eyewall and the radial gradient of (potential) vorticity outside of the hurricane core is known as the beta of a hurricane vortex. Hence, the skirt of the non-zero radial gradient in the azimuthal-mean potential vorticity field is called the "beta-skirt." *Terwey and Montgomery* (2008) proposed, using a 3-D high-resolution mesoscale numerical model simulation of Hurricane Ivan (2004), the Beta-Skirt Axisymmetrization (BSA) hypothesis.

Sporadic convection is hypothesized to occur within the beta-skirt. The strength of this convection is limited by factors including the strength of the convective available potential energy, convective inhibition (CIN), and the mean filamentation time scale (τ_{fil}) (*Wang et al., 2013*). CIN is the amount of energy needed to break through the thermodynamic "ceiling" that prevents spontaneous convection, and τ_{fil} is the amount of time it takes to shear convective cells. Deep convection occurs with a filamentation time greater than 30 minutes, substantial CAPE, and low CIN.

The perturbation vorticity and kinetic energy produced by this convection is then axisymmetrized upscale into the azimuthal-mean flow through the process of anisotropic cascade. An axisymmetrization process occurs when asymmetric disturbances, such as vorticity anomalies generated by convection, are tilted in the direction of the basic-state shear so that the energy is being transferred from the asymmetries to the symmetric circulation (*Peng et al., 2008*). The anisotropic (directionally dependent) upscale energy cascade is the process in which the energy of smaller-scale anomalies is absorbed by the large-scale circulation.

After some time, this axisymmetrization of sporadic deep convection forms a low-level jet within the beta-skirt. Once this jet is large enough, the Wind Induced Surface Heat Exchange (WISHE) process (*Yano and Emanuel, 1991*) intensifies it. The WISHE process states that an increase in winds results in an increase in the amount of latent and sensible heat fluxes. This makes the low-level air favourable for convection, thus creating more convection. This positive feedback cycle will continue to intensify the convection in the beta-skirt and eventually a secondary eyewall will form. The beta-skirt mechanism requires that a hurricane have a large enough potential vorticity skirt.

Qiu et al. (2010) suggested that both the beta-skirt and outward propagating vortex Rossby waves result in an eyewall replacement. They proposed that the beta-skirt axisymmetrization establishes an extensive beta skirt and that vortex Rossby waves propagating radially outward from the primary eyewall to a certain radius

will result in the formation of a secondary eyewall.

2.1.2.2 *Vortex Rossby Wave Propagation*

Vortex Rossby waves (VRWs), first presented by *Montgomery and Kallenbach* (1997), are coherent potential vorticity perturbations that flow from the primary eyewall that are superimposed on a symmetric vortex with a mean radial potential vorticity gradient (*Chen and Yau, 2001*). They have similar characteristics to Rossby waves. *Chen and Yau* (2001) showed, using a non-hydrostatic mesoscale model, that both potential vorticity bands and cloud bands are strongly coupled. They also found that potential vorticity anomalies that are located in and at the top of the boundary layer work with friction to produce upward motions, and that these upward motions result in the formation of cloud bands. The flow properties of these potential vorticity bands were found to be consistent with predictions of vortex Rossby wave theory. The characteristics for wavenumber-1 and -2 VRWs, as described by *Wang* (2002) include:

- Waves are well coupled with asymmetries in eyewall convection and play an important role in the life cycle of a hurricane.
- Waves transport angular momentum from the eyewall to the eye.
- Waves accelerate the tangential winds in the eye while decelerating the tangential wind in the eyewall.

These characteristics suggest that VRWs play an important role in the inner core dynamics of a hurricane. Therefore, using two high-resolution (WRF-ARW) 3-D full physics hurricane simulations of Hurricane Katrina (2005) and Hurricane Rita (2005) and comparing the results to RAINEX (2005), *Abarca and Corbosiero* (2011), showed that VRWs travelled radially outward from the inner vortex to a certain radius. At this radius, the radial group velocity tends to be zero and the waves concentrate angular momentum. This radius is called the stagnation radius and it is at this location where strong outer rainbands most frequently occur (*Wang, 2002*).

Angular momentum concentration at the stagnation radius will generate a secondary tangential wind maximum, resulting in the formation of a secondary eyewall. This is known as the Vortex Rossby Wave Stagnation Radius hypothesis. This hypothesis requires a radial gradient of potential vorticity that is conducive for VRW propagation.

Using a 2-D barotropic dry model, *Martinez and Yau* (2010), showed that asymmetric disturbances located outside of a vortex and within a large vorticity skirt formed concentric rings of vorticity, which resulted in a secondary wind maximum near a critical radius. It was suggested that because the enhanced vorticity formed near a critical radius that this process was due to VRW dynamics and propagation.

2.1.2.3 *Potential Vorticity Accumulation*

Using high-resolution cloud-resolving simulations of real topical cyclones (Hurricane Katrina (2005) and Hurricane Rita (2005)), and comparing the results to RAINEX (2005) observations, *Judt and Chen* (2010) presented that convectively generated potential vorticity accumulation in the outer rainbands played an important role in the secondary eyewall formation of Hurricane Rita. A secondary eyewall did not form in Hurricane Katrina.

According to the study, sporadic convection in the outer rainbands that generates potential vorticity is projected onto the azimuthal-mean state. How sporadic convection generates an organized potential vorticity band is still a research question, but it alters the wind field by generating a jet, or secondary horizontal tangential wind, at or below the level of maximum heating. This jet has been observed by studies such as *Barnes et al*. (1983) and *Hence and Houze* (2008). This jet can enhance surface fluxes and strengthen the convection in the outer rainbands and further increase the secondary maximum tangential wind. The outer rainbands eventually coalesce and form a secondary eyewall. The results of the paper were not able to determine why a secondary eyewall occurred in Hurricane Rita and not in Hurricane Katrina or what caused the sporadic convection to form in the secondary eyewall formation region. It was suggested that the

shape of the outer rainbands might play a role in the secondary eyewall formation. It is an area of concentration for their future research, but it has been addressed in this thesis.

2.1.2.4 *Unbalanced Dynamics in the Hurricane Boundary Layer*

The theories mentioned previously were performed in terms of a balanced framework (axisymmetric and gradient wind balance), but hurricanes may include important unbalanced (imbalance in gradient wind) boundary layer processes. Using a very high-resolution (0.67 km) 3-D full physics hurricane simulation, *Wang et al*. (2013) showed that as a hurricane reached certain intensity, a positive net radial force associated with the intensifying hurricane develops a secondary maximum net radial force over the secondary eyewall formation region. The positive net radial force induces a secondary maximum convergence zone, resulting in a secondary maximum updraft at the secondary eyewall region over the top of the boundary layer. The coupling of this vertical updraft and the hurricanes secondary circulation inflow organizes the moist convection and results in a secondary eyewall. This theory is in agreement with *Huang et al*. (2012) on the process of the unbalanced boundary layer structural changes that occur during a secondary eyewall formation process. These structural changes include:

- A broadening of tangential wind due to the inward radial flow of absolute angular momentum within and just above the hurricane boundary layer.
- Increase in boundary layer inflow underneath the broadened tangential wind.
- The development of a convergence zone above and within the boundary layer outside the primary eyewall.

These structural changes have been confirmed by other studies including *Abarca and Montgomery* (2013) and *Kepert* (2013). As of this date, no other studies have looked at the importance of the net radial force and its corresponding boundary layer convergence for secondary eyewall formation. However, using an axisymmetric nonlinear slab boundary layer model, *Abarca and Montgomery* (2013) demonstrated that boundary dynamics alone could lead to the development of a

secondary tangential wind maximum. Contrary to this, *Menelaou et al*. (2014) showed, using a 3-D regional model including boundary layer physics with thermal forcings excluded, that boundary layer physics alone did not lead to a secondary eyewall. Rather, the paper suggested that the boundary layer most likely contributed, but did not initiate, the formation of the secondary eyewall.

2.1.2.5 *Outer Rainband Latent Heating*

Eliassen (1951) found that surface convergence due to friction and heat transfer to the air sustains a hurricane's secondary circulation and the Sawyer-Eliassen equation was developed to diagnose the response of heating and/or momentum forcing to the secondary circulation. Using the Sawyer-Eliassen diagnoses and tangential momentum budget analysis, *Zhu and Zhu* (2015) calculated outer rainband heating for balanced tropical cyclone-like vortices on an f-plane. They showed that outer rainband diabatic heating is crucial to the development of the secondary tangential wind maximum. The process proposed involves sporadic convection in the outer rainband region that generates convergence of radial inflow and accelerates tangential wind at the base of the convection. These processes result in an increase of moisture in the low troposphere, which favours the development of low-level convection, and according to the Sawyer-Eliassen diagnoses, this low-level convection can lead to convergence of radial flow and acceleration of tangential winds in the upper boundary layer (*Zhu and Zhu, 2015*). This positive feedback leads to the transport of more moisture into the outer rainbands and the enhancement of surface evaporation. Both of these processes strengthen outer rainband convection, and once this convection reaches certain strength relative to the primary eyewall (approximately 10%), the outer rainbands will then strengthen and coalesce into a secondary eyewall. This paper was unfortunately not able to answer the question of what causes the sporadic convection in the outer rainband region to form and begin the feedback process.

There have been several studies conducted on the importance of diabatic heating. For example, *Menelaou et al*. (2014) showed that even in the absence of

boundary layer processes, the potential vorticity generated by sustained rainband-like heating organized into a potential vorticity ring. This ring then formed a secondary tangential wind maximum. The magnitude of this rainband-like heating was found to be important for secondary eyewall formation: if the magnitude was too low a secondary eyewall did not form. Using a 3-D non-hydrostatic linear model, *Moon and Nolan* (2010), showed that the secondary tangential wind maximum was a result of diabatic heating in the rainbands. If the diabatic heating lasted long enough, the secondary wind maximum wrapped around the entire storm vortex and a secondary eyewall developed.

The hypothesized mechanisms that initiate a secondary eyewall are vast, and many of them compete with one another. Further evaluations of these hypotheses are needed to advance our understanding of the underlying mechanisms that initiate ERCs. Several of the mentioned theorized mechanisms are examined in this thesis using a 3-D full physics model hurricane simulation.

Chapter 3: Methodology

3.1 Real Case Study

Although ERCs can occur in many intense hurricanes, it is difficult to simulate them. Hurricane Danielle (2010) was chosen because the ERC happened and it was actually simulated. Hurricane Danielle (2010) is also a best-case scenario for studying the internal dynamics of ERCs. Danielle formed a secondary eyewall in the middle of the ocean, in the absence of any external mechanisms such as topography. This suggests that Hurricane Danielle's secondary eyewall was the result of environmental and internal workings alone.

Hurricane Danielle (2010) began as a tropical depression on August 21st, 2010 and strengthened into a tropical storm 12 hours later on August 22nd. Danielle developed into a Category 2 hurricane on the Saffir-Simpson scale on August 23rd. A decrease in wind shear due to the weakening of a subtropical ridge over the central Atlantic led to a strengthening of Danielle on August 26th that continued into August 27th. Danielle reached her peak intensity as a Category 4 hurricane on August 27th around 1800 UTC with a sustained maximum wind speed of 115 knots and a pressure of 942 hectopascals (hPa). A gradual weakening of Danielle occurred on August 28th due to an evolving eyewall replacement cycle (Figure 6).

Danielle continued to weaken in response to a southwesterly shear ahead of a mid- to upper-level trough moving off the east coast of the United States (*Kimberlain, 2010*). This trough also caused Danielle to turn sharply northeastward towards cooler waters and she eventually weakened back to a tropical storm on August 30th.

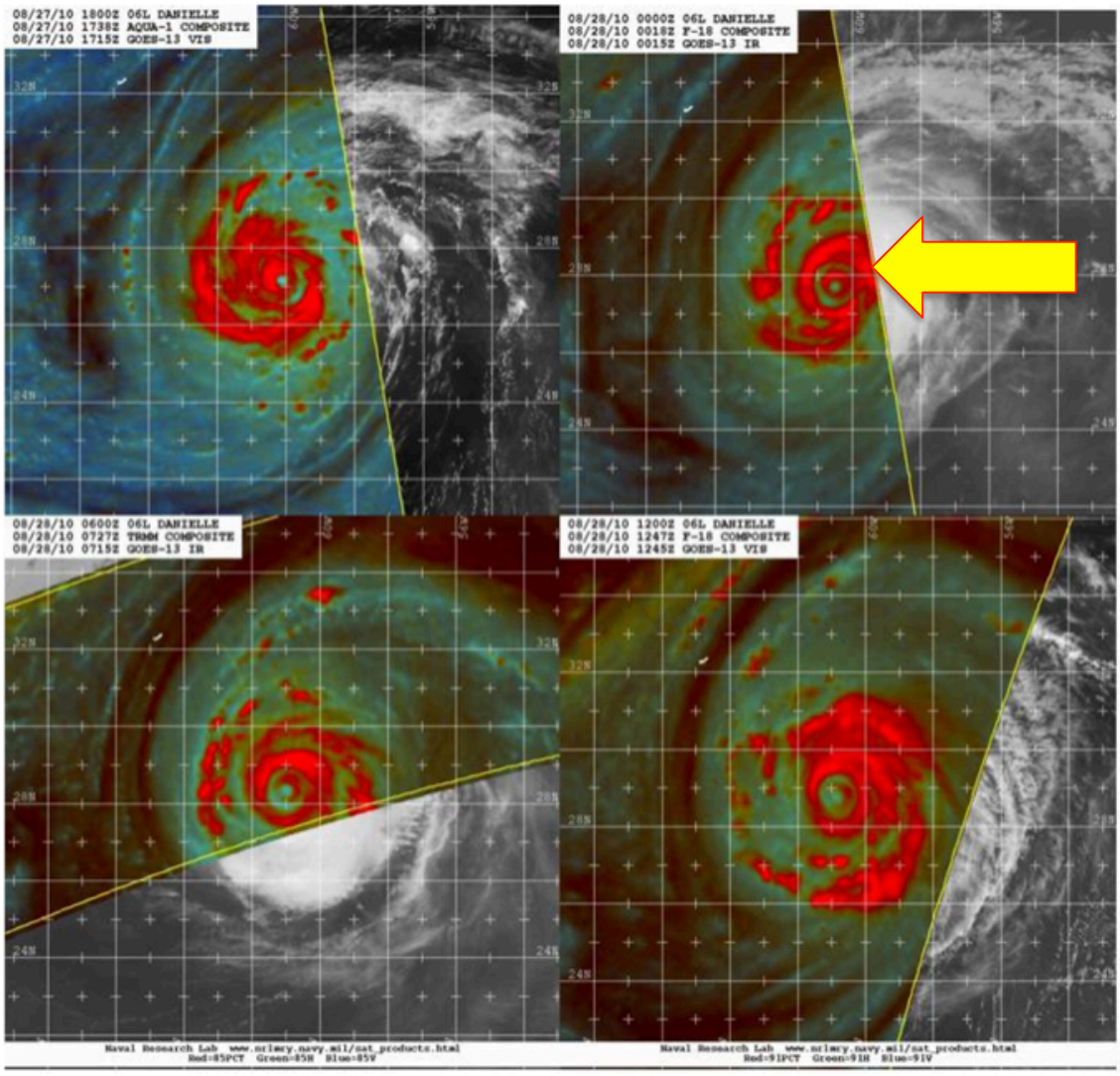

Figure 6: Microwave satellite images showing the eyewall replacement (arrow) of Hurricane Danielle (2010) on August 27th and 28th (*Kimberlain, 2010*)

3.2 Model Configuration

The WRF model, version 3.3 with the ARW dynamic solver, was used for all simulations performed in this study. The WRF model is a latest-generation mesoscale numerical weather prediction and atmospheric simulation system that is used internationally for research and operational applications (*Skamarock et al., 2008*). It is a fully compressible, non-hydrostatic model that has been used successfully for both real

and idealized tropical cyclone simulations.

The WRF-ARW model uses a terrain-following dry hydrostatic-pressure vertical coordinate and Arakawa C-grid staggering to solve the primitive equations (*Skamarock et al., 2008*). The model physics in the ARW solver includes microphysics, cumulus parameterization, surface models, planetary boundary layer, and atmospheric radiation.

All simulations contain quadruple nested, storm-following square domains with horizontal resolutions of 36, 12, 4 and 1.33 km, respectively (Figure 7) and grid points of 320x210, 133x133, 199x199 and 241x241. There are 35 vertical levels with the lowest 8 levels below 1 km height. The microphysics scheme used was a WRF double-momentum six-class scheme (*Chen and Dudhia, 2000*). This scheme includes 6 hydrometeor species: water vapour, cloud water, rain, ice, snow, and graupel. The planetary boundary layer (PBL) scheme was the YSU scheme. The Kain-Fritsch scheme (*Kain and Fritsch, 1990*) was used to represent sub-grid scale convective cumulus parameterization in the two outer-most domains.

The Noah land-surface model and the Monin-Obukhov surface layer scheme were used for surface physics. The Rapid Radiative Transfer Model and the Goddard radiation schemes were used for longwave and shortwave radiation, respectively. Horizontal diffusion was determined using a 2-D Smagorinsky turbulence closure scheme while the vertical turbulent diffusion was handled by the PBL scheme. All simulations were run for 5 days.

The model was initialized on August 25th, 2010 at 1200 UTC when Danielle was already at hurricane strength. The National Centre of Atmospheric Research (NCAR) Ensemble Kalman Filter (EnKF) mean analysis data were used for the initial conditions. The simulations performed in this study differ by changing the value of the Smagorinsky constant in the equation for horizontal eddy diffusivity.

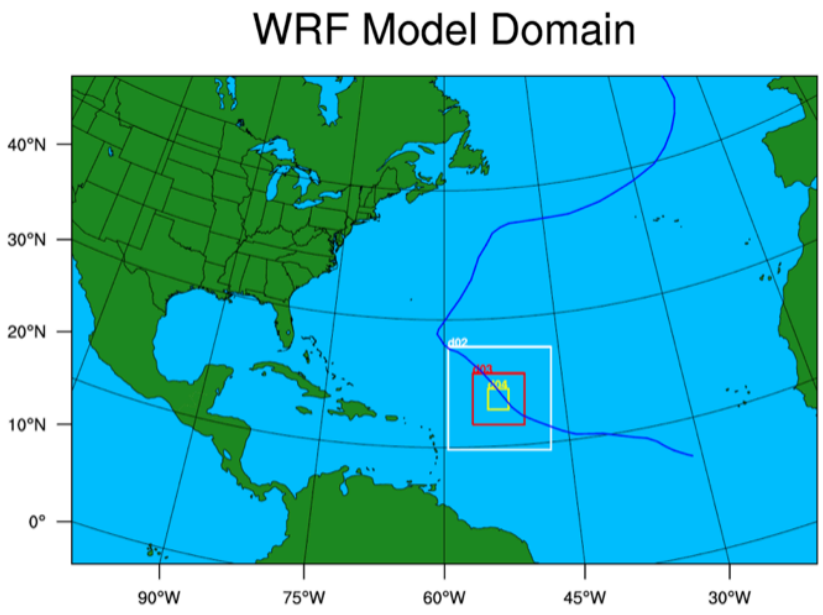

Figure 7: Domain set-up for simulated Hurricane Danielle (2010). D01=36 km, D02=12 km, D03=4 km, and D04=1.33 km

3.3 Horizontal Turbulent Mixing in WRF-ARW Model

The turbulent transport of energy and momentum have to be parameterized using a sub-grid scale parameterization scheme because the horizontal grid spacing of operational models for hurricane simulations and forecasting are generally much larger than the size of turbulent eddies (*Zhang and Montgomery, 2012*). The parameterization of turbulence is usually achieved through an eddy diffusion closure model. As mentioned in *Section 3.2*, a 2-D Smagorinsky closure scheme was used in the simulations performed.

Turbulent flows contain a wide range of length and time scales and numerical models with finite resolutions can only explicitly describe the flows with length scales larger than the grid size. The effects of sub-grid scale motions on the resolved scales can be parameterized in analogy with molecule degrees of freedom in the kinetic theory of gases, in which the momentum fluxes are linearly dependent upon the rate of strain of the resolved scales (*Meneveau, 2010*). Currently, the best-known sub-grid scale parameterization scheme is the one developed by *Smagorinsky* (1963) and it is used in the

WRF-ARW model.

In the Smagorinsky scheme, the momentum change due to horizontal diffusion can be written as:

$$\partial_t u = \partial_x \tau_{11} + \partial_y \tau_{12} \quad 3.1$$

$$\partial_t v = \partial_x \tau_{12} + \partial_y \tau_{22} \quad 3.2$$

The indices 1 and 2 represent the physical coordinates x and y respectively. ∂_t, ∂_x, and ∂_y are the partial derivatives with respect to t, x, and y. The stress tensor τ can be written as follows:

$$\tau_{11} = -K_h D_{11} \quad 3.3$$

$$\tau_{22} = -K_h D_{22} \quad 3.4$$

$$\tau_{12} = -K_h D_{12} \quad 3.5$$

The deformation tensor D is defined as:

$$D_{11} = 2\partial_x u \quad 3.6$$

$$D_{22} = 2\partial_y v \quad 3.7$$

$$D_{12} = \partial_y u + \partial_x v \quad 3.8$$

The horizontal eddy viscosity K_h is then defined as:

$$K_h = l_h^2 [0.25(D_{11} - D_{22})^2 + D_{12}]^{1/2} \quad 3.9$$

$$l_h^2 = C_s^2 l^2 \quad 3.10$$

C_s is the Smagorinsky constant, $l = \Delta x$ is the grid distance, which varies with the domain, and l_h is the mixing length scale. The value of l was not changed in the simulations performed, but the value of the Smagorinsky constant was varied to change the magnitude, and thus test the sensitivity of the simulations to changes in the horizontal mixing length. This is discussed in the next chapter.

Chapter 4: Model Simulation Sensitivity

To study the sensitivity of ERCs to horizontal turbulent mixing parameterization, simulations were performed where the Smagorinsky constant, C_s, was replaced by the values of 0.0, 0.25 and 1.0. These sensitivity experiments are named CS0, CS025, and CS1, respectively. The CS0 experiment implies that there is no horizontal turbulent mixing, CS1 experiment involves much stronger horizontal turbulent mixing, and CS025 — the control run — is the standard value used in most hurricane simulations. The sensitivity experiments are 5-day simulations, but the analysis period focuses only on the ERC period in each.

As it turns out, only two of the simulations formed an ERC. But the question is: *why?* To answer this, it is important to first look at the differences in these simulations.

4.1 Sensitivity to Horizontal Mixing Length

Varying the horizontal turbulent mixing doesn't change the track, but does change the intensity of the hurricane significantly. Figure 8 shows the track accuracy of the simulations, each compared with the best track data.

The simulated hurricane tracks follow Danielle's best track very well and experience little deviation. The only major difference occurs when Danielle turned sharply northeastward due to an external force (a deep trough formed over the east coast of the United States (Figure 9)), and the simulations were unable to match the sharp northeastward turn.

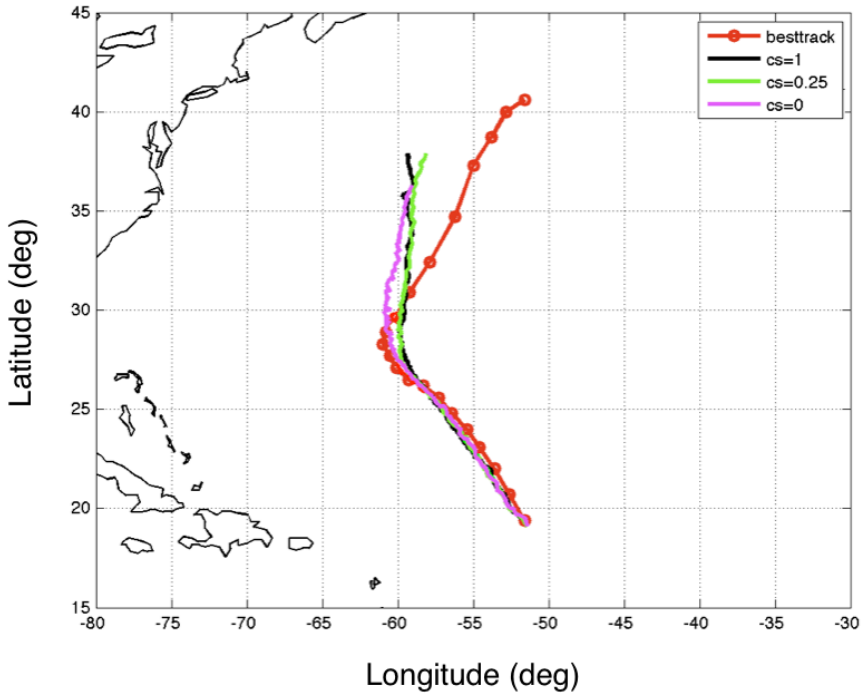

Figure 8: Hurricane Danielle (2010) best track (red) and simulated tracks for Cs=0 (magenta), Cs=0.25 (green), and Cs=1 (black)

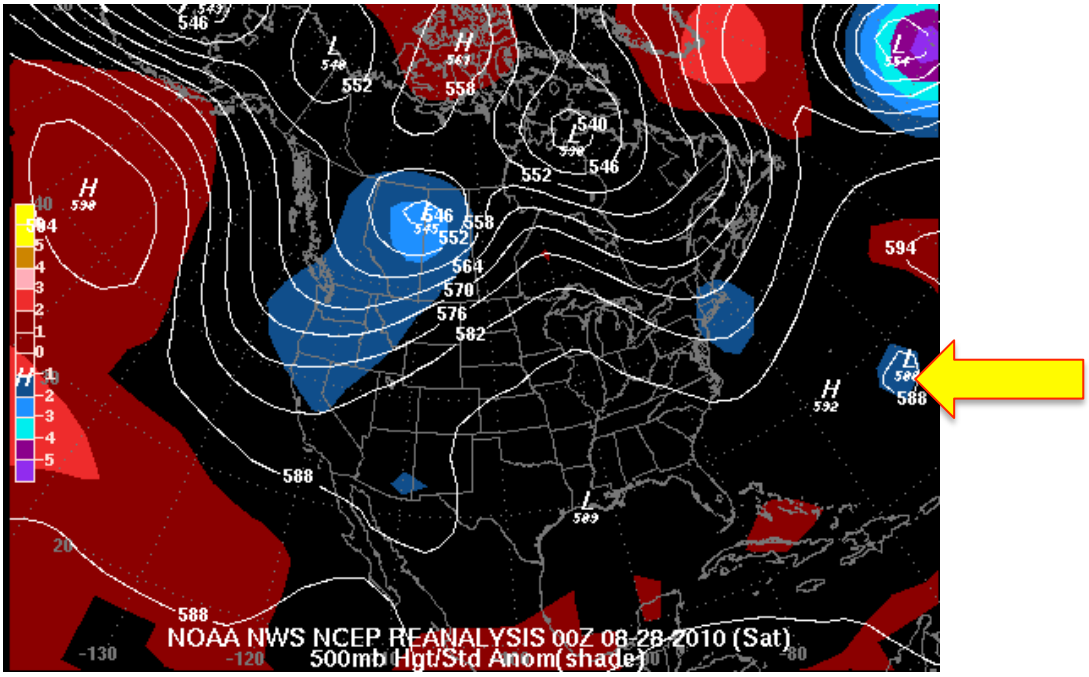

Figure 9: NOAA NWS NCEP Reanalysis Data Display by NCEP on August 28th, 2010 at 00 UTC. Image is a 500-millibar height map displaying the upper-level trough and even Hurricane Danielle (2010) can be seen (arrow).

Figure 10 shows the time series of minimum sea-level pressure and maximum wind speed of simulated Hurricane Danielle (2010) and that the intensity is quite sensitive to changes in C_s. For example, in CS0, the simulated hurricane is very strong with a minimum wind speed of speed of 73 ms^{-1} and a minimum sea-level pressure of 912 hPa. In CS025, the maximum wind speed is 64 ms^{-1} and a minimum pressure of 930 hPa, and in CS1 the maximum wind is 55 ms^{-1} with a minimum sea-level pressure of 948 hPa. Table 1 summarizes these main characteristics in determining a hurricane's categorical strength.

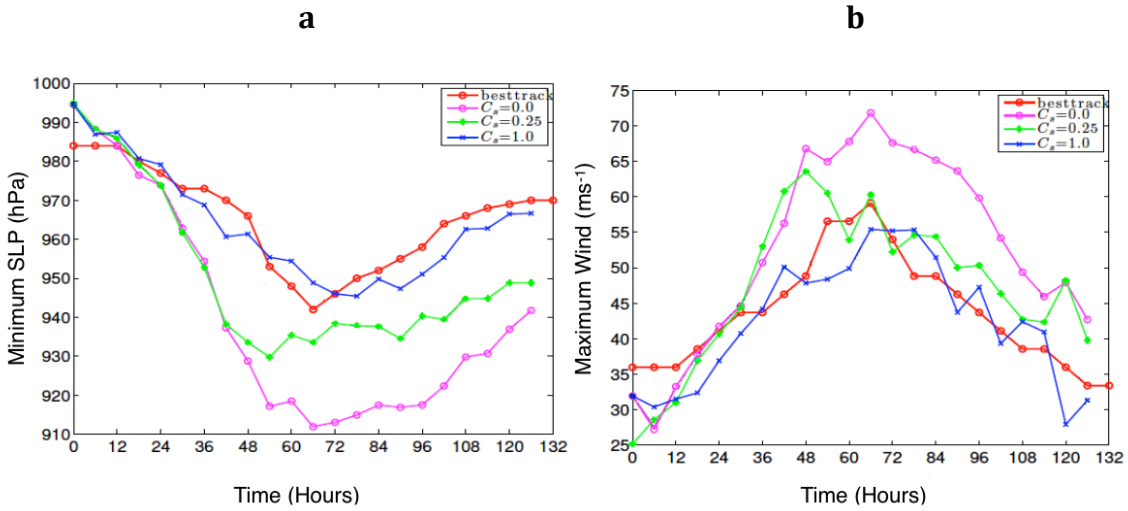

Figure 10: Hurricane Danielle (2010) best track (red) and simulated (a) minimum sea-level pressure (hPa) and (b) maximum tangential wind speed (ms^{-1}) for Cs=0 (magenta), Cs=0.25 (green), and Cs=1 (blue)

Simulation	Maximum Wind	Minimum Pressure	Hurricane Category
CS025	**124 knots** (64 ms^{-1})	**930 hPa**	**4**
CS0	**141 knots** (73 ms^{-1})	**912 hPa**	**5**
CS1	**107 knots** (55 ms^{-1})	**948 hPa**	**3**
Danielle (2010)	**115 knots** (59 ms^{-1})	**942 hPa**	**4**

Table 1: The maximum wind speed (ms^{-1}), minimum sea-level pressure (hPa), and hurricane strength based off the Saffir-Simpson scale for Cs=0. Cs=0.25, Cs=1, and real Hurricane Danielle's (2010) best track

Surprisingly, the CS1 run was the most accurate in simulating Hurricane Danielle's strength. The reason this is surprising is because CS1 substantially increased the horizontal turbulence mixing and it did not develop an eyewall replacement cycle. However, the CS025 simulation was also fairly accurate in simulating Hurricane Danielle's strength, while the CS0 simulation produced a very low minimum sea-level pressure and large maximum sustained wind speed, thus a much stronger Category 5 hurricane — a hurricane strength that Danielle never reached. The width of the convective bands in each simulation should also be noted. The simulations CS0 and CS025 both had very narrow convective bands, while the CS1 contained very wide bands (*see* Figure 12). This difference is the result of changes in the horizontal turbulent mixing parameter and may be of importance in the formation of a hurricane's secondary eyewall.

The time that the eyewall replacements occurred in CS025 and CS0 were also quite sensitive to horizontal mixing length. The secondary eyewall started to occur around the 38th hour in CS025 around 40-70 km radii — corresponding to a date of August 27th at 0200 UTC. However, in CS0, the secondary eyewall appeared around 40-70 km radii at the 55th hour, which corresponds to a date of August 27th at 1800 UTC. In reality, Hurricane Danielle formed a secondary eyewall on August 28th at 0000 UTC around 60 km radius. While both simulations produced an eyewall replacement cycle too early, CS0 with no horizontal turbulent mixing was early by just 6 hours, while CS025 produced the eyewall replacement cycle about 22 hours early. This suggests, once again, that hurricane intensity and simulation accuracy are sensitive to changes in horizontal turbulent mixing length.

4.2 Hurricane Boundary Layer Structure

To understand the structure of the hurricane boundary layer, the vertical structure of the radial winds, azimuthal winds, and cloud water mixing ratio are examined. As seen in Figures 11 and 12, increases in horizontal mixing length for turbulent diffusion yields a less compact structure. In CS0 and CS025, the boundary layer radial inflow does not extend very high (shallower). However, it is much deeper in CS1. What's more, the radial

inflow and outflow layer for CS1 are both stronger, but the convergence near the eyewall is a lot weaker due to the elevated radial outflow layer. Why this vertical radial flow is shallower in CS0 and CS025 will be an area of future research.

The CS0 and CS025 simulated Hurricane Danielle (2010) both show a well-developed eye (two local maxima) in the azimuthal winds. It is more defined in CS0, with an eyewall radius approximately 20-25 km surrounded by strong and compact surface winds. However, in CS1, simulated Hurricane Danielle (2010) shows weaker winds surrounded by a loosely formed eyewall with a radius of approximately 40-45 km.

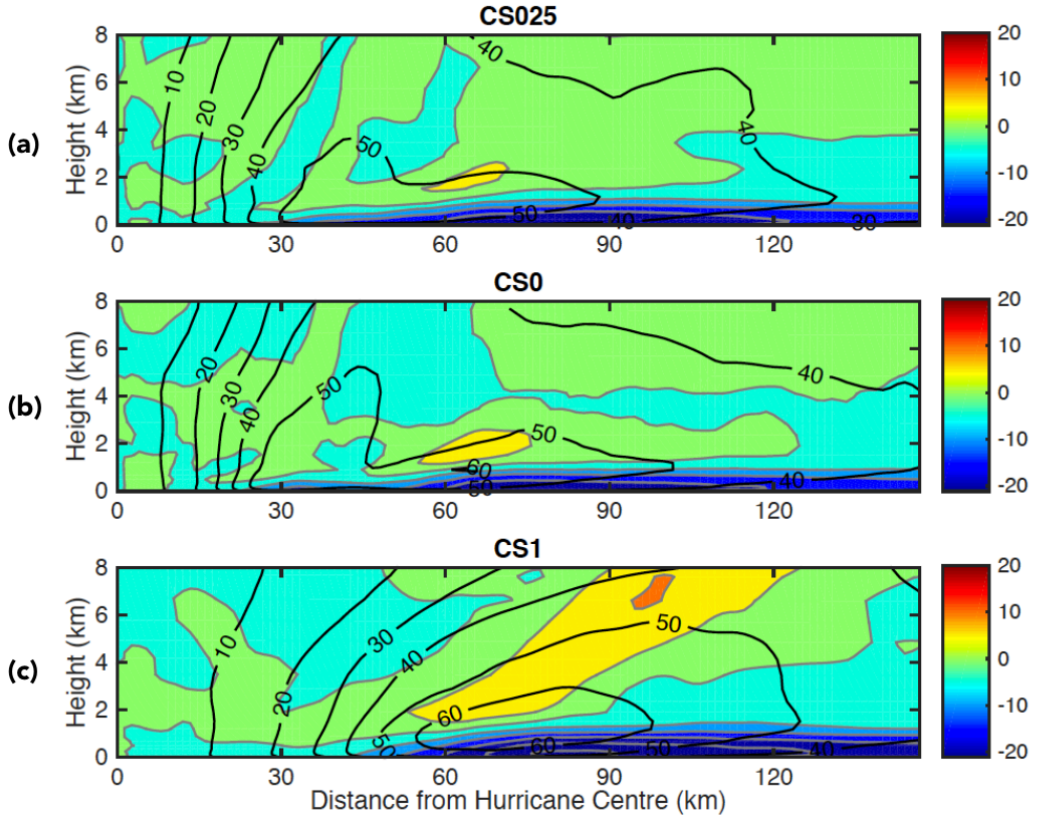

Figure 11: Vertical cross-section of azimuthal-mean radial velocity (ms^{-1}) overlaid with azimuthal-mean tangential wind (ms^{-1}) (black lines) for simulated Hurricane Danielle (2010) for (a) Cs=0.25 at t=38 hours (during ERC), (b) Cs=0 at t=55 hours (during ERC), and (c) Cs=1 at t=55 hours.

What is important to note is that a concentric secondary eyewall clearly appears in

the simulations CS0 and CS025 and that the primary eyewall is also narrower in CS0, but wider and flatter in CS1. The image of simulated cloud water mixing ratio at 1 km height shows the secondary concentric eyewall for Hurricane Danielle (2010) for t=55 hours for CS0 and t=38 hours for CS025 (arrows). For CS0, the timing is roughly the same for when the secondary eyewall was observed in real Hurricane Danielle (2010), but was still fairly close to CS025. The vertical cross-section of tangential wind also shows the second wind maximum outside of the primary wind maximum.

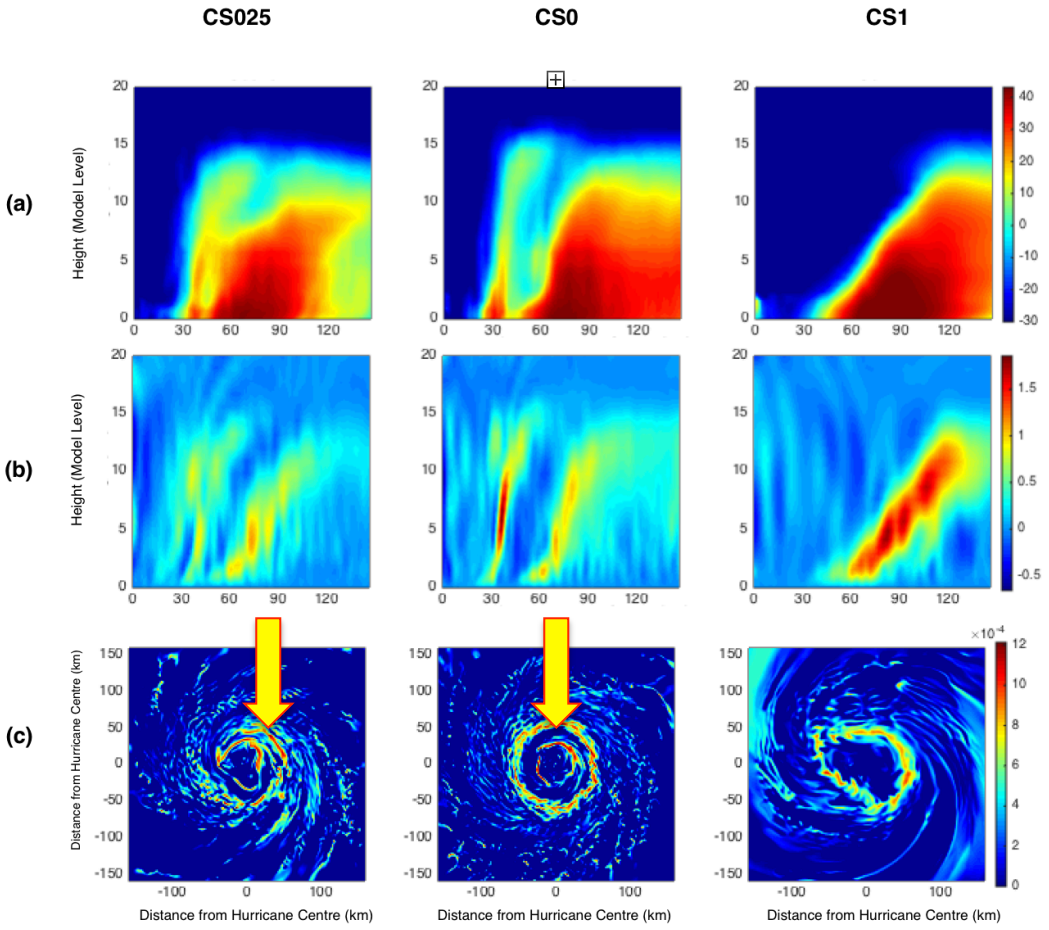

Figure 12: Vertical cross-sections of azimuthal-mean (a) radar reflectivity (dBZ), (b) vertical wind (ms^{-1}), and (c) horizontal cross-section of cloud water mixing ratio ($g\ kg^{-1}$) at ~1 km height for Cs=0.25 at t=38 hours, Cs=0 at t=55 hours, and Cs=1 at t=55 hours.

Analysis of environmental conditions, structure, dynamics, and the mechanisms discussed in *Chapter 2* led to the following hypothesis:

Reducing the magnitude of the horizontal turbulent mixing length reduces the amount of diffusion in the x-y plane, resulting in more narrow convective rainbands and eyewall. These narrow bands result in a drier outer environment due to enhanced subsidence between the rainbands that is forced by diabatic heating. This makes the rainbands more circular and they begin to evolve toward an eyewall-like structure (*Houze et al., 2005*). The reduced horizontal turbulent mixing also results in more shallow radial inflow near the surface. The radial inflow brings higher angular momentum air inward, which increases the tangential winds outside of the primary eyewall, broadening the tangential wind. A secondary tangential wind maximum, or low-level jet, forms due to vertical advection in the circular rainband region. If the radial inflow is shallower, then the low-level jet is closer to the surface. This jet further increases evaporation, diabatic heating, convection, and radial inflow. The rainbands coalesce and a secondary eyewall begins to form.

Chapter 5: ERC Hypothesis

The following sections test the hypothesis discussed in *Chapter 4* by diagnosing environmental conditions, circularity, as well the mechanisms discussed in *Chapter 2*.

5.1 Environmental Conditions and Circularity

A strong horizontal moisture gradient within a moist hurricane surrounded by a dry outer environment may confine a hurricane into a pattern that causes the outer rainbands to have high circularity, promoting the formation of a secondary eyewall (*Ortt, 2007*). A conceptual model of this idea is shown in Figure 13. We suggest that the ERCs in our simulation developed in a moist hurricane that is not only surrounded by a drier outer environment, but the rainbands are also circular because of this moisture distribution.

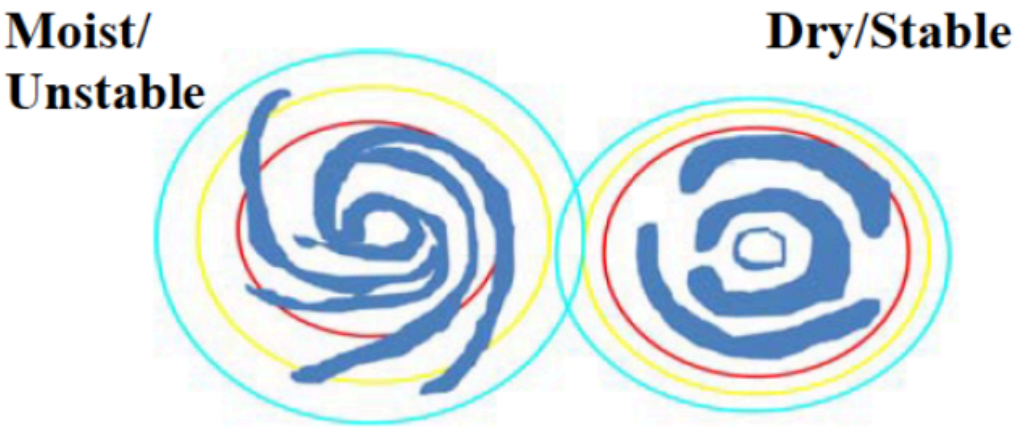

Figure 13: Conceptual model of moisture gradient and hurricane rainband structure. Relatively weak gradient (left) may favour extended spiral rainbands. A strong moisture gradient (right) may confine rainbands at a particular radius. Areas inside of the red circle represents very moist and unstable environment while areas outside of the light blue circle represents dry and stable. The dark blue shapes are hurricane rainbands (*Ortt, 2007*)

Images of relative humidity, water vapour mixing ratio, and radar reflectivity are shown (Figure 14) to examine the internal and external moisture environment, and in turn, circularity of each hurricane simulation. High relative humidity is an important

ingredient in the strength of a hurricane. Dry air, especially at midlevels, impedes the development of a hurricane because it causes the evaporation of liquid water. Since evaporation is a cooling process, it reduces the warm-core of the hurricane and limits the vertical growth of convection. All simulations have high relative humidity within the hurricane.

A hurricane with a less moist outer region — due to narrow convective bands — as seen in the CS0 simulation, may have a stronger atmospheric stability that is less favourable for deep convection far from the centre of the hurricane. A moist outer environment is unstable, such as with CS1. This may allow for the rainbands to extend further from the centre of the hurricane, and therefore result in a less circular shape. The condition for a strong moisture gradient appears to be satisfied.

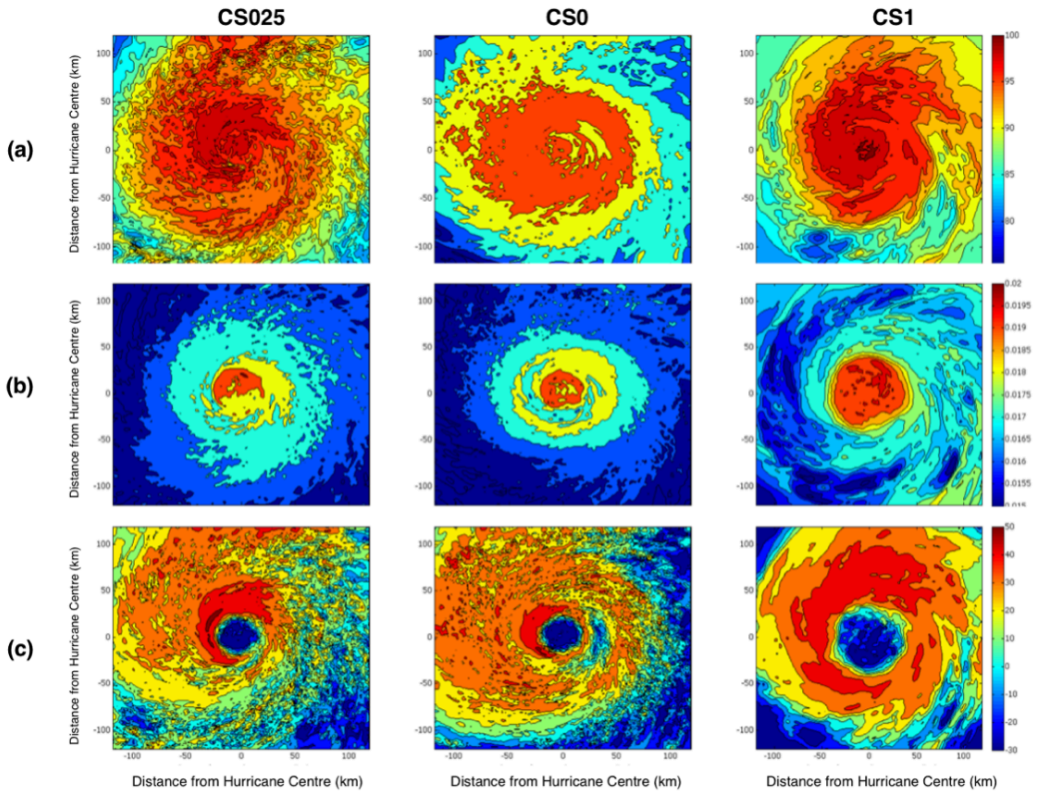

Figure 14: Horizontal plots at ~1 km height of (a) relative humidity (%), (b) water vapour mixing ratio (g kg^{-1}), and (c) radar reflectivity (dBZ) for Cs=0.25 at t=38 hours, Cs=0 at t=55 hours, and Cs=1 at t=55 hours.

The shape of the rainbands in CS0 simulation is noticeably more circular than the other two simulations, and smaller-scale precipitation and convective elements are captured. In CS1, the convective bands are very wide; therefore it does not capture any of the small-scale convection. The outer rainbands are also not very circular. The condition of circular outer rainbands for ERC formation appears to be satisfied based on the figures discussed.

5.2 Broadening of the Tangential Wind Field

The broadening of the tangential wind field is an important process in ERC formation. What the term "broadening" means is that the strength of the hurricane tangential winds begins to expand outwards in the radial direction (away from the centre of the hurricane). What causes this expansion is currently under debate, however, we propose it is the result of a balance response to diabatic heating in the outer rainbands.

The location of the heating in relation to the radius of the tangential maximum wind speed was suggested to be important for the "efficiency" — the amount of temperature warming compared to the amount of latent heat released — of diabatic heating (*Smith and Montgomery, 2016*). When the heating is inside the radius of maximum wind (RMW), it is more efficient in developing a rapid increase in tangential wind.

According to the images (Figure 15), an increase of diabatic heating in the secondary eyewall formation may occur slightly before the radial broadening of the tangential winds, and also inside of the newly forming radius of the secondary maximum. This suggests that our idea of tangential broadening could in fact be a balance response to diabatic heating. It begins to form in the outer rainbands then further acts to increase the newly forming secondary tangential wind maximum.

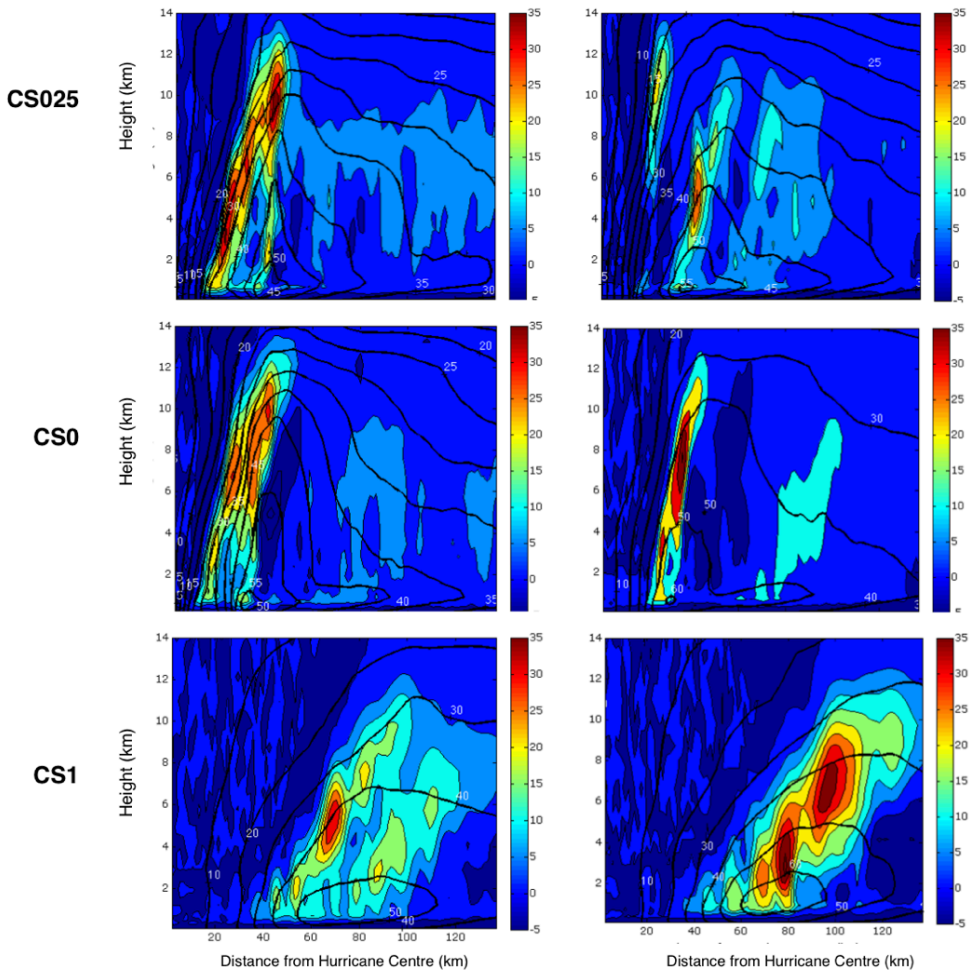

Figure 15: Radius-height plots of azimuthal-mean diabatic heating (K hr^{-1}) overlaid with azimuthal-mean tangential wind (ms^{-1}) for Cs=0.25 at t=30 hours and t=35 hours, Cs=0 at t=45 hours and t=55 hours, and Cs=1 at t=45 hours and t=55 hours.

5.3 Potential Vorticity Generation

Convectively generated potential vorticity (PV), or potential vorticity asymmetries, if enough are generated, can develop a similar structure to outer spiral rainbands, which are dominated by wavenumber-1 components (*Wu and Braun, 2003*). But how are these asymmetries generated? *Judt and Chen* (2010) conducted a potential vorticity budget analysis of Hurricane Rita (2005) and Hurricane Katrina (2005) to determine how the secondary potential vorticity and wind maxima developed. The budget is written as follows:

$$\frac{\partial \bar{P}}{\partial t} = -\nabla \cdot \left(\overline{\boldsymbol{v}}\bar{P} - \frac{\bar{Q}}{\rho}\overline{\boldsymbol{\omega}} + \overline{\boldsymbol{v}'P'} - \frac{1}{\rho}\overline{Q'\boldsymbol{\omega}'} \right) \quad 5.1$$

Potential vorticity $\bar{P}$ is defined as

$$\overline{P} = -g\overline{\zeta_a \cdot \nabla\theta} \quad 5.2$$

and where

$\overline{\boldsymbol{v}} = Velocity\ vector$

$\bar{Q} = Diabatic\ heating$

$\rho = Density$

$\overline{\boldsymbol{\omega}} = Vorticity\ vector$

$t = Time$

$g = Gravity$

$\overline{\zeta_a}$ = Absolute vorticity

$\bar{\theta} = Potential\ temperature$

The overbars denote azimuthal average and the primes denote the perturbations, or deviations, from the azimuthal average. The left hand side of Equation 5.1 is the local rate of change of azimuthally averaged potential vorticity, while the terms on the right-hand side of the equation include sources and sinks. The first term is the PV flux due to the mean vortex circulation and the second term is the divergence of the azimuthally averaged diabatic heating and the azimuthally averaged vorticity vector. The third term is a potential vorticity flux due to the asymmetric potential vorticity and the fourth term is the potential vorticity generation by the perturbation diabatic heating and vorticity. The perturbation diabatic heating and vorticity are a result of convective-scale elements (*Judt and Chen, 2010).*

According to the budget equation, only the mean and perturbation terms of Q and ω generate potential vorticity. The other terms are just local sources and sinks — they do not generate potential, they only redistribute it. Figure 16 shows the generation rates due to the azimuthal and perturbation components from the potential vorticity budget equation.

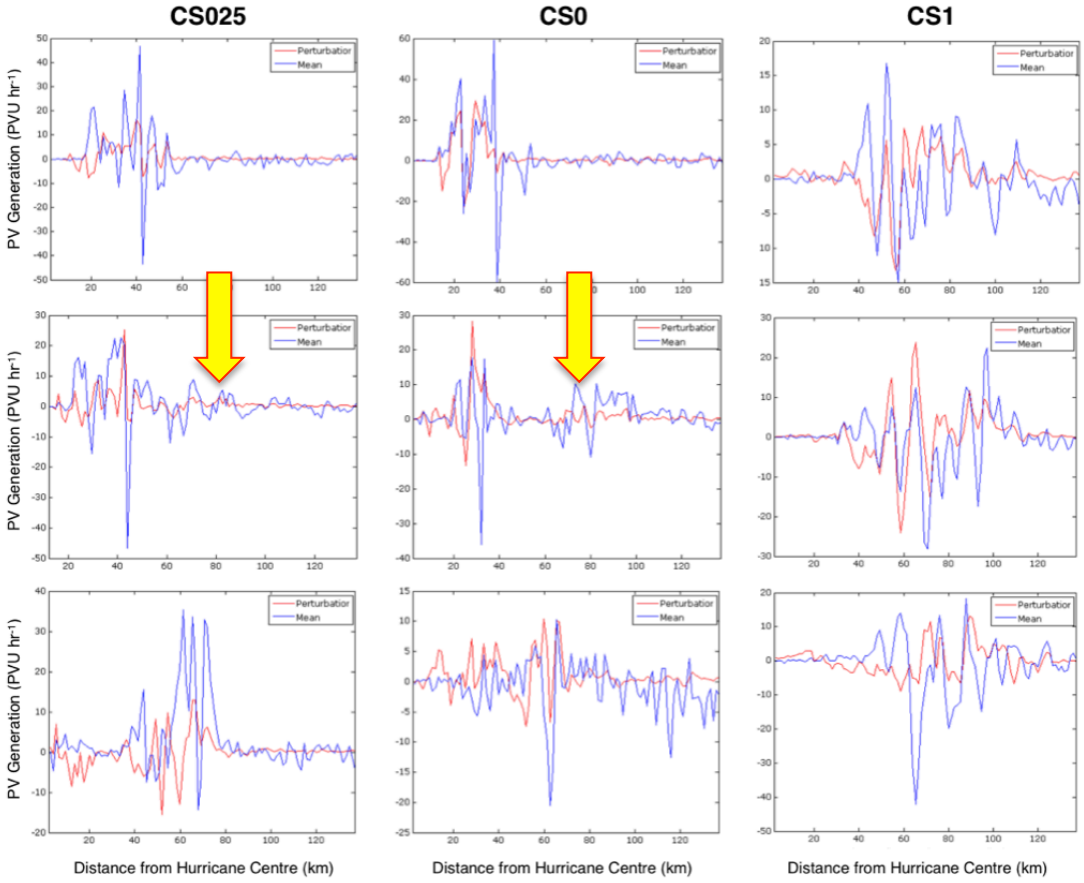

Figure 16: 5-hour averaged potential vorticity rates (PVU hr^{-1}) before, during and after ERC at ~2 km height due to the azimuthally-averaged component (blue) and the perturbation component (red) calculated from the second and fourth terms in the potential vorticity budget equation for Cs=0.25 at t=25-30 hours, t=33-38 hours, and t=45-50 hours, Cs=0 at t=35-40 hours, t=50-55 hours, and t=65-70 hours, and Cs=1 at t=35-40 hours, t=50-55 hours, and t=65-70 hours.

Potential vorticity in the eyewall region is predominantly generated by the mean heating and vorticity term (blue) prior to ERC, which can be seen from the figures. However, the potential vorticity in the rainband region during the secondary eyewall formation is generated by both the mean term and perturbation term. As the primary eyewall begins to weaken, potential vorticity generated by the mean term decreases. As a result, the convection in the inner eyewall weakens. The location of the secondary eyewall can be seen (arrows) in both the mean and perturbation generation terms, and as

time evolves, the secondary maximum potential vorticity begins to look similar to the original eyewall — with an increase in the mean generation terms and a decrease in the perturbation generation terms.

To evaluate where these anomalies are generated — whether they are an extension of the primary eyewall or if they develop separately from it— it is important to look at vortex Rossby waves. To examine the roles of VRWs in ERCs, the potential vorticity field is divided into azimuthally symmetric and asymmetric parts. The asymmetric components, or PV perturbations, are decomposed into different azimuthal wavenumbers by Fourier decomposition. According to *Abarca and Corbosiero* (2011), potential vorticity variance, or enstrophy, is best to use in identifying VRW activity. Enstrophy is a measure of the intensity of the integral of vorticity and it is proportional to the sum of squares of the wave amplitudes. The azimuthal-mean enstrophy is determined by the following equation:

$$Enstrophy = \frac{1}{2}\sum_{n=1}^{\infty}[q_n(r,z)]^2 \qquad 5.3$$

where

$q_n(r,z) = Amplitude\ of\ wavenumber\ n$

$r = Radius$

$z = Vertical\ height$

Figure 17 displays radius-height cross-sections of azimuthal-mean potential vorticity and amplitude of perturbation potential vorticity of azimuthal wavenumbers 1 through 3 (WN1, WN2, and WN3) and Figure 18 shows the enstrophy.

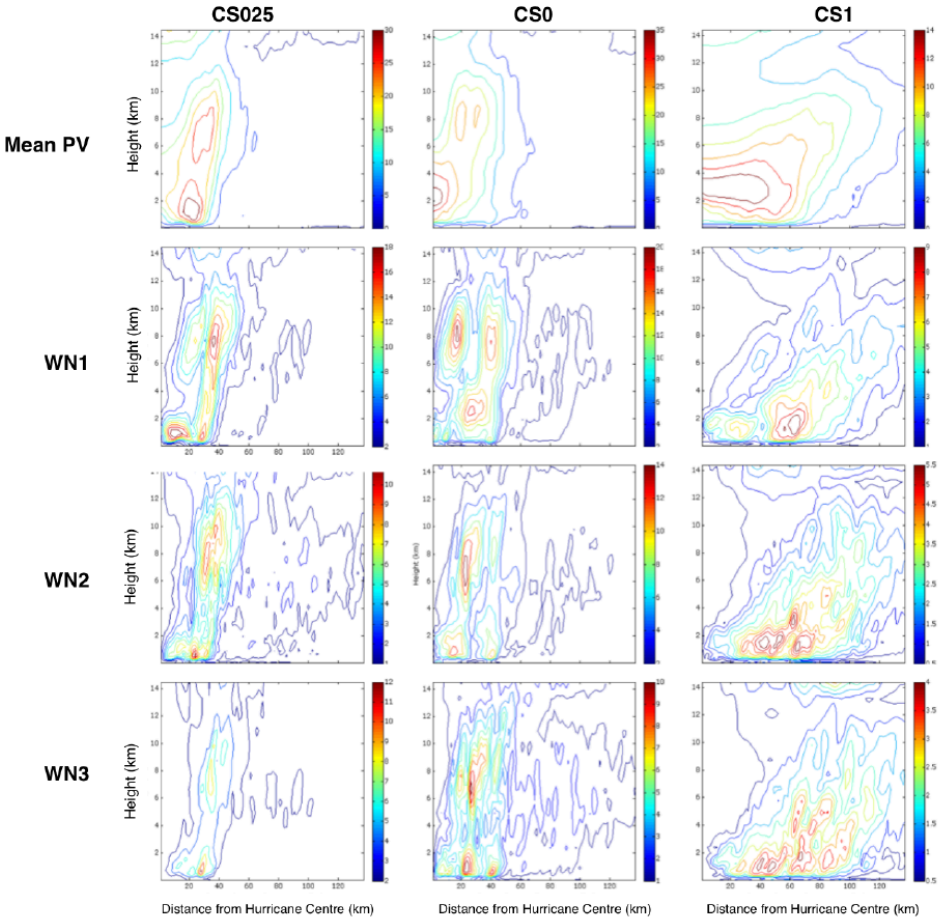

Figure 17: Radius-height cross-sections of 5-hour azimuthally averaged potential vorticity amplitude (PVU) and low wavenumber (1-3) potential vorticity perturbation amplitude (PVU) for Cs=0.25 at t=25-30 hours, Cs=0 at t=35-40 hours, and Cs=1 at t=35-40 hours.

We can see from these two sets of images that pockets of wavenumber-1 potential vorticity anomalies, the largest contributor to the variance, are being produced in the secondary eyewall formation region separated from the primary eyewall by the moat — the region between the eyewall and outer rainbands that is often associated with relatively light rain. This suggests that the potential vorticity in the outer rainband region is not generated through the outward propagation of VRWs in our simulations. The enstrophy images also show that there is trivial activity outside the primary eyewall. We also believe that the potential vorticity anomalies generated through sporadic convection are the result of an already occurring initiating mechanism.

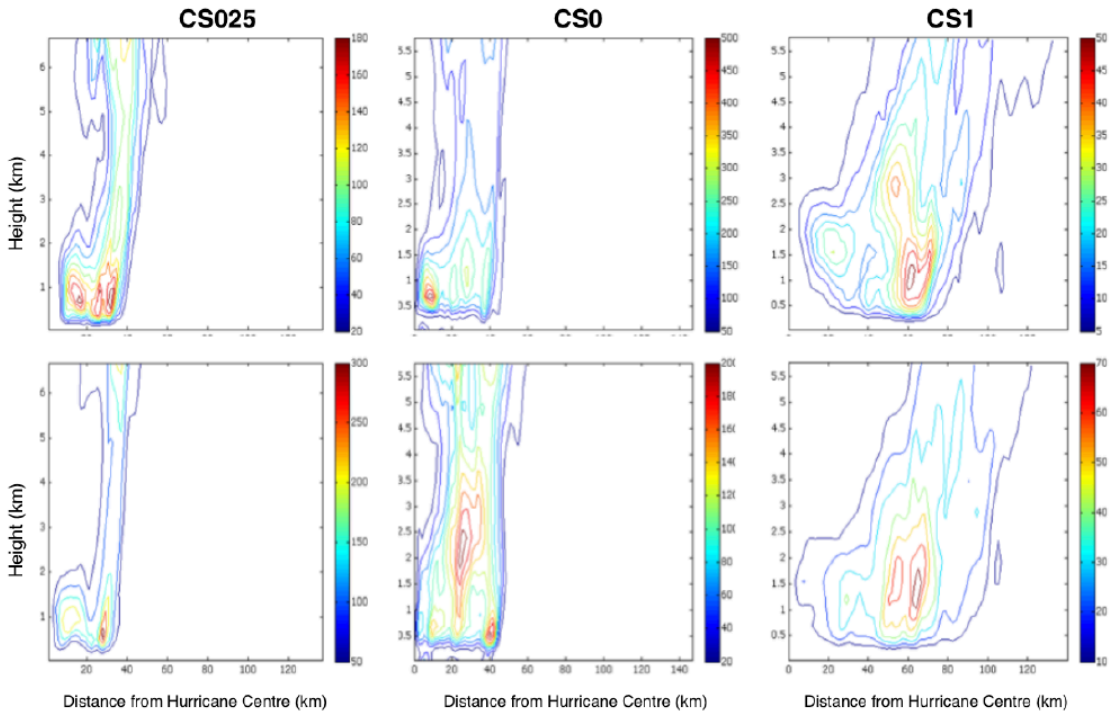

Figure 18: Radius-height cross-sections of 5-hour average azimuthally averaged potential vorticity variance (PVU^2) for Cs=0.25 at t=25-30 hours and t=33-38 hours, Cs=0 at t=35-40 hours and t=50-55 hours, and Cs=1 at t=35-40 hours and t=50-55 hours.

5.4 Axisymmetrization

As discussed in *Chapter 2*, an axisymmetrization process occurs when asymmetric disturbances, such as vorticity anomalies generated by convection, are tilted in the direction of the basic-state shear. The study by *Terwey and Montgomery* (2008) examined the role of the hurricane beta skirt and filamentation time, and their importance in initiating the formation of a secondary eyewall by an axisymmetric process. To evaluate their potential importance, the formula for the calculation of effective beta (β) and filamentation time (τ_{fil}) from *Rozoff et al.* (2006) are used:

$$\beta = -\left(\frac{\partial \bar{P}}{\partial r}\right)\left(\frac{\bar{\xi}}{\bar{P}}\right) \qquad 5.4$$

$$\tau_{fil} = \left[-\left(\frac{\bar{V}}{r}\right)\left(\frac{\partial \bar{V}}{\partial r}\right)\right]^{1/2} \qquad 5.5$$

$$\bar{\xi} = f + 2\frac{\bar{V}}{r} \qquad 5.6$$

where

$\bar{P} = Potential\ vorticity$

$\bar{\xi} = Intertial\ parameter$

$\bar{V} = Tangential\ wind$

$f = Coriolis\ parameter$

$r = Radius$

Overbars represent azimuthal-averages. The negative sign on effective beta is to represent that the increase in potential vorticity with decreasing radius is associated with positive effective beta. If effective beta is positive, the energy of vortex Rossby waves will propagate outward. If effective beta is negative, the energy of VRWs will propagate inward, and if filamentation time is less than 30 minutes, then there is not enough time for deep convection to occur, which inhibits hurricane convective growth.

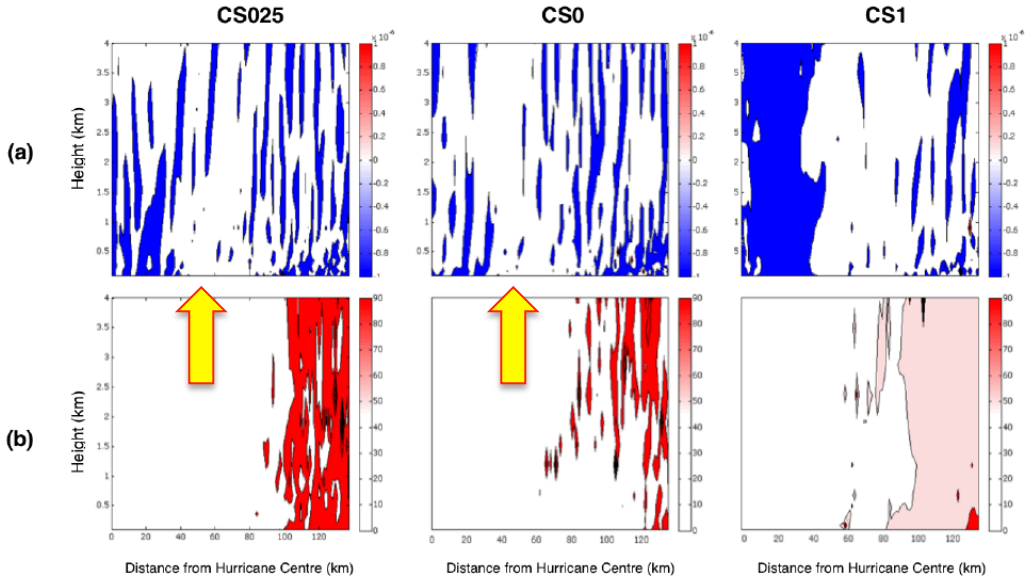

Figure 19: Radius-height cross-sections of 5-hour averaged azimuthally averaged (a) effective beta (10^{-6} m^{-1} s^{-1}) and (b) filamentation time (min) for Cs=0.25 at t=25-30 hours, Cs=0 at t=35-40 hours, and Cs=1 at t=35-40 hours

The results of the analysis (Figure 19) show that there is a negative effective beta region within the primary eyewall (arrows), which suggests that the gradient of azimuthal-mean potential vorticity is not conducive for VRW propagation toward the secondary eyewall formation region. Not only that, filamentation time is less than 30 minutes almost everywhere within the hurricane, except in the far outer regions, which also indicates that the Beta-Skirt Axisymmetrization mechanism is not active in our simulations.

5.5 Low-Level Jet Formation

Convectively generated potential vorticity alters the wind field by generating a jet, or secondary horizontal tangential wind, at or below the level of maximum heating. According to *Barnes et al.* (1983), air spiralling inward toward the storm centre is subjected to an overturning circulation as it encounters increased potential vorticity. The overturning tilts the convective cells, stretching, and vertically transporting vorticity so the convergence of the vertical flux of vorticity strengthens the vorticity anomaly (*Hence and Houze, 2008*) within the secondary eyewall formation region resulting in a low-level jet.

This jet can enhance surface fluxes and strengthen the convection in the outer rainbands and, hence, further increase the secondary maximum tangential wind. This jet has been observed by several studies as mentioned in *Chapter 2*. To show the formation of the low-level jet, Figure 20 displays the change in azimuthally averaged tangential wind from hour "0" (T-23 for CS025, T-40 for CS0, and T-40 for CS1), for three, 5-hour intervals. It is easier to see small changes to a large field, such as tangential winds, by examining the field as a difference from a reference field (*Terwey and Montgomery, 2008*).

It is clear from the images that there is a positive jet forming (arrows), associated with the strengthening of convection in the outer rainbands. This further intensifies with time and moves radially inward toward the secondary eyewall formation region.

However, as time progresses, the inner section begins to weaken, which is associated with the weakening of the primary eyewall due to the formation of outer ring convection. The results suggest that the formation of the low-level jet may be satisfied.

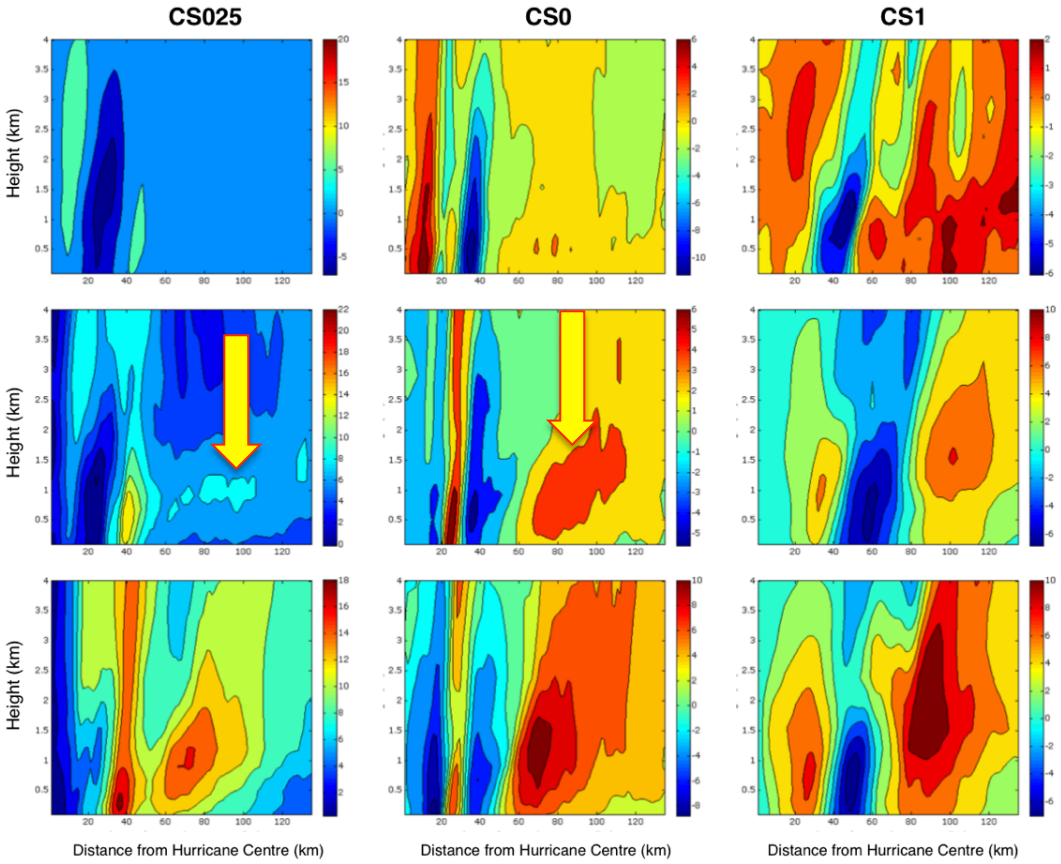

Figure 20: Change in azimuthal-mean tangential wind (ms^{-1}) from hour "0" for Cs=0.25 at t=25, 33, and 38 hours, Cs=0 at t=45, 50, and 55 hours, and Cs=1 at t=45, 50 and 55 hours

5.6 Hurricane Boundary Layer

The hurricane boundary layer controls the radial distribution of moisture, vertical motion, absolute angular momentum and the structure of the unbalanced flow (*Wang et al., 2013*). Wang et al. (2013) analyzed the structure and evolution of the net radial force within the hurricane boundary layer. The azimuthal-mean tangential and radial momentum equation and continuity equation with the Boussinesq approximation in cylindrical coordinates were used in determining the net radial force:

$$\frac{\partial \bar{U}}{\partial t} + \bar{U}\frac{\partial \bar{U}}{\partial r} + \bar{W}\frac{\partial \bar{U}}{\partial r} - \frac{\bar{V}^2}{r} - f\bar{V} = -\frac{1}{\rho}\frac{\partial \bar{p}}{\partial r} + \bar{F}_r + \bar{F}_{reddy} \quad 5.7$$

$$\frac{\partial \bar{V}}{\partial t} + \overline{U\zeta_a} + \bar{W}\frac{\partial \bar{V}}{\partial r} = \bar{F}_\lambda + \bar{F}_{\lambda eddy} \quad 5.8$$

$$\frac{1}{r}\frac{\partial (r\bar{U})}{\partial r} + \frac{\partial \bar{W}}{\partial z} = 0 \quad 5.9$$

The analysis of the radial forces in the hurricane boundary layer was determined by the following process by first combining (5.7) and (5.9):

$$r\times[Eq.5.6] + \bar{U}\times[Eq.5.8] \quad 5.10$$

Then, taking a depth average from the surface to the top of the boundary layer, H (assumed constant at 500 metres):

$$\bar{U}_b = \left(\frac{1}{H}\right)\int_0^H \bar{U}dz \quad 5.11$$

$$\bar{V}_b = \left(\frac{1}{H}\right)\int_0^H \bar{V}dz \quad 5.12$$

$$\bar{U}' = \bar{U} - \bar{U}_b \quad 5.13$$

Assuming a steady state approximation, the net radial force equation is:

$$\frac{1}{r}\frac{\partial r(\bar{U}_b^2)}{\partial r} = -\frac{1}{H}\int_0^H \frac{1}{\bar{\rho}}\frac{\partial \bar{p}}{\partial r}dz + \frac{1}{H}\int_0^H \frac{\bar{V}^2}{r}dz + f\bar{V}_b + \frac{1}{H}\int_0^H \bar{F}_{fric}dz + \frac{1}{H}\int_0^H \bar{F}_{reddy}\,dz - \frac{1}{rH}\int_0^H \left(\frac{\partial (r\bar{U}^2)}{\partial r}\right)dz - \frac{\overline{WU}}{H}_{z=H} \quad 5.14$$

where

$\bar{U} = Radial\ wind$

$\bar{V} = Tangential\ wind$

$\bar{W} = Vertical\ wind$

$f = Coriolis\ parameter$

$\bar{\rho} = Density$

$\bar{p} = Pressure$

$\bar{F}_r, \bar{F}_\lambda = Friction\ in\ radial\ and\ azimuthal\ directions, respectively$

$\zeta_a = Absolute\ vertical\ vorticity$

$\bar{F}_{reddy}, \bar{F}_{\lambda eddy}$

$= Eddy\ momentum\ flux\ in\ radial\ and\ azimuthal\ directions, respectively$

$r = Radius$

$H = Height\ of\ the\ hurricane\ boundary\ layer$

$t = Time$

The right hand side of Equation 5.14, in order, starting with the first, is the pressure gradient force, followed by the centrifugal force, the Coriolis force, friction forces, azimuthally asymmetric eddy flux, azimuthally symmetric eddy flux, and the radial momentum flux from the boundary layer top. The sum of all these terms is the net radial force.

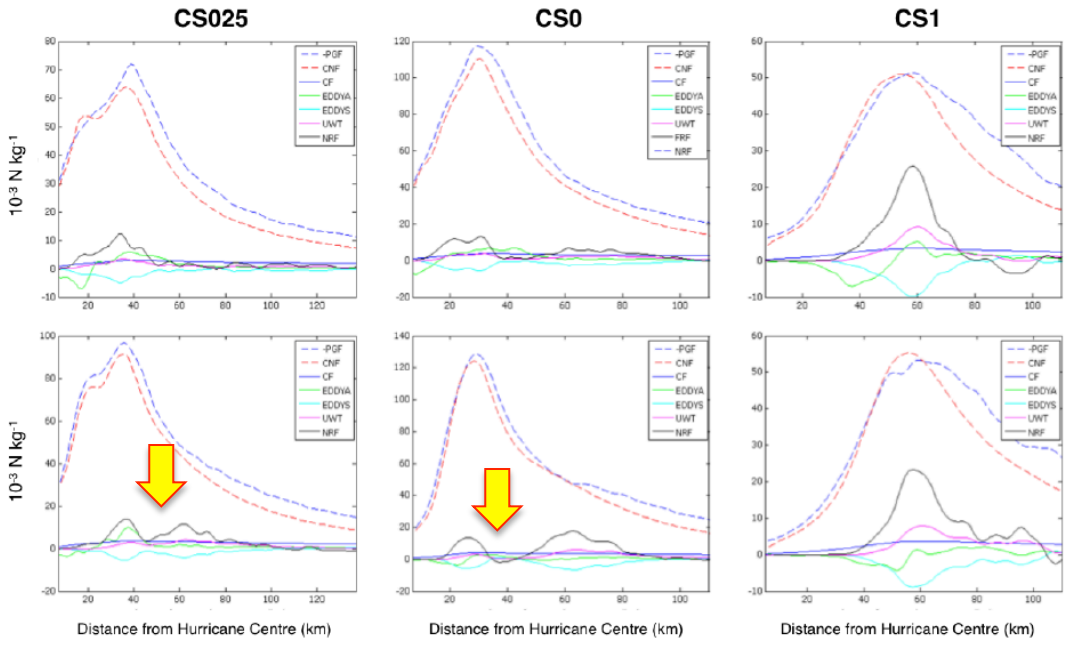

Figure 21: Radial profiles of time averaged boundary layer depth azimuthally averaged pressure gradient force (-PGF), centrifugal force (CNF), Coriolis force (CF), azimuthally asymmetric eddy flux (EDDYA), azimuthally symmetric eddy flux (EDDYS), and radial momentum flux at the top of the boundary layer (UWT) and the net radial force (NRF) for Cs=0.25 at t=25-30 hours and t=33-38 hours, Cs=0 at t=35-40 hours and t=50-55 hours, and Cs=1 at t=35-40 hours and t=50-55 hours, respectively

Negative pressure gradient force is plotted in Figure 21. The two strongest forces are the negative pressure gradient force and centrifugal force, but they generally cancel each other because of their opposite sign. That indicates that the remaining terms are small, but they still contribute to the net radial force term. Friction terms were excluded as they are small and the simulations were not set to output these terms. However, the exclusion does not affect the results. Two peaks of net radial force are seen (arrows), just as seen in the paper by *Wang et al*. (2013). Similarly, a decreasing net radial force region exists between the two positive regions, which is associated with the moat.

The results (Figure 21) are interesting as no ERC forms in the CS1 simulation, but the net radial force value is quite large. It would be expected that such a large net radial force would initiate a secondary maximum convergence zone at some time during the simulation. However, that does not happen. This suggests that a positive net radial force is a result of an already occurring process that is initiating uplift and ascent and is not an initiating mechanism of ERC. This suggests that the net radial force mechanism, although it may be active, is not the initiating mechanism in our simulations.

5.7 Diabatic Heating Sensitivity Experiments

Sensitivity experiments were performed to test the importance of diabatic heating to the secondary eyewall formation process. A run with the Smagorinsky constant set to 0.0 and diabatic heating reduced by 25% (CS0_NEW) was performed, as well as a run with the Smagorinsky constant set to 1.0 and diabatic heating increased by 50% (CS1_NEW).

In CS0_NEW, a secondary eyewall did not form, while in the CS1_NEW run, a secondary eyewall may have formed (Figure 22). However, it is very late in the simulation and very far away from the centre of the hurricane (arrow) — making it very difficult to diagnose. These results illustrate the importance of diabatic heating to the secondary eyewall formation process. In the original CS0 simulation, a very clear and strong secondary eyewall formed around the 55th hour. However, when diabatic heating was reduced by 25%, the convection was strongly reduced and the hurricane was not able to form a secondary maximum of tangential wind.

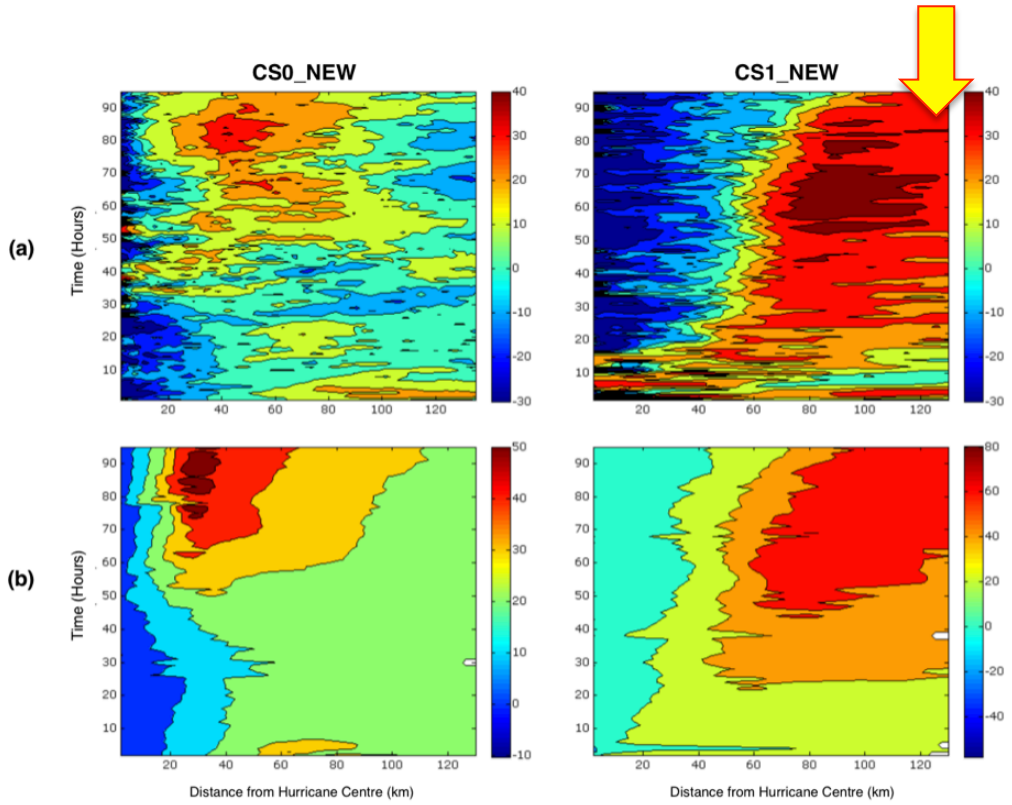

Figure 22:Radius-time plots of azimuthally averaged (a) radar reflectivity (dBZ) at ~1 km height and (b) tangential velocity (ms^{-1}) at ~1 km height for CS0_NEW and CS1_NEW

So what does all this mean? We have shown that not only does horizontal turbulent mixing greatly impact the size and shape of the convective rainbands — inner and outer — but also diabatic heating also plays an important role in the formation of a secondary eyewall.

Chapter 6: Summary and Future Scope

6.1 Summary

We used the WRF-ARW model to study the sensitivities of horizontal turbulent mixing on hurricane eyewall replacement cycles by simulating a real case study of Hurricane Danielle (2010). If the horizontal mixing length l_h from the 2-D Smagorinsky closure scheme is reduced by setting the Smagorinsky constant C_s to a small value, the intensity of the simulated hurricane increases. It was also observed that the structure of the simulated hurricane, and the formation of a secondary eyewall and subsequent eyewall replacement cycle vary strongly with changes to C_s. When C_s was set to 0.0 (no horizontal turbulent mixing), the simulated hurricane became very intense with a maximum wind speed of 73 ms^{-1} and a minimum sea-level pressure of 912 hPa. The simulation also captured the small-scale convective processes (which is believed to be essential in the secondary eyewall formation process) and underwent a clear eyewall replacement cycle.

When C_s was set to 0.25, the simulated hurricane was not as strong, but an eyewall replacement cycle, although not as clear to see, still occurred and was also able to capture the small-scale convective elements. When C_s was set to 1.0 (maximum mixing within these simulations), the simulated hurricane was much weaker, the convective bands were very wide, and an ERC did not occur. These results show that the WRF-ARW model of simulated ERCs of Hurricane Danielle (2010) is sensitive to changes in horizontal turbulent mixing.

In order to diagnose why only two of the simulations produced an ERC, five theories on the formation mechanism that initiate an ERC were evaluated. The results of the diagnoses revealed that the proposed mechanisms (summarized in the table below) by *Terwey and Montgomery* (2008), *Judt and Chen* (2010), *Abarca and Corbosiero* (2011), and *Wang et al.* (2013) were not the initiating mechanism of ERCs in our simulations. On the other hand, the hypothesized mechanism proposed by and *Zhu and Zhu* (2015) on the

importance of diabatic heating in the outer rainbands was found to be important in our simulations. However, we believe enhanced diabatic heating is the result of our proposed ERC mechanism.

Author	Internal Dynamics	Active?
Terwey and Montgomery (2008)	Potential vorticity is filamented and axisymmetrized upscale within a hurricane's beta-skirt	No
Judt and Chen (2010)	Potential vorticity is projected onto the azimuthal-mean flow which generates a low-level jet	No
Abarca and Corbosiero (2011)	Outward propagating vortex Rossby waves stall at a stagnation radius and concentrate angular momentum	No
Wang et al. (2013)	Positive net radial force in an intensifying hurricane develops a second positive net radial force inducing a secondary maximum convergence zone	No
Zhu and Zhu (2015)	Outer rainband diabatic heating and convection results in a positive feedback process and once this convection reaches a critical strength a secondary eyewall forms	Maybe

Table 2: Summary of five theories on the initiating mechanism of ERCs

Given the results of the initiating mechanisms diagnosed in our simulations, a new mechanism was proposed for ERC formation. Reducing the magnitude of the horizontal turbulent mixing results in more narrow convective rainbands. These narrow rainbands result in a drier outer environment due to enhanced subsidence between the rainbands forced by diabatic heating, making the rainbands more circular. The reduced horizontal turbulent mixing also results in a shallower radial inflow near the surface and a low-level jet forms due to vertical advection in the circular rainband region. This jet further

strengthens and a secondary eyewall forms.

Two sensitivity experiments were also conducted to test the importance of diabatic heating in our simulations. The first involved reducing diabatic heating by 25% in a simulation that had initially produced an ERC, while the second increased it by 50% in a simulation that initially did not produce an ERC. The results of the sensitivity experiments further emphasized the importance of diabatic heating to the eyewall replacement process.

To summarize this thesis, the eyewall replacement process is sensitive to changes in the horizontal mixing length as is evident by varying the Smagorinsky constant. Several hypotheses on the proposed initiating mechanisms of ERCs were evaluated against our simulations and only one was found to be potential candidates for an initiating mechanism. A hypothesis was then proposed on the initiating mechanism of ERC that addresses the initial radial broadening of the tangential wind field.

6.2 Future Scope

The results presented in this thesis promote research opportunities in the field of hurricane eyewall replacement dynamics and hurricane forecasting:

1) Further study can be completed to evaluate the proposed hypothesis with other real case hurricane simulations that produce a secondary eyewall.
2) Further study can be completed to determine why the radial inflow layer is shallower when horizontal turbulent mixing is reduced.

References

Abarca, S. F., and K. L. Corbosiero, 2011: Secondary eyewall formation in WRF simulations of Hurricane Rita and Katrina (2005). *Geophys. Res. Lett.,* **38,** L07802, doi:10.1029/2011GL047015.

Abarca, S. F., and M. T. Montgomery, 2013: Essential dynamics of secondary eyewall formation. *J. Atmos. Sci.,* **70,** 3216-3230.

Barnes, G. M., E. J. Zipser, D. Jorgensen, and F. Marks Jr., 1983: Mesoscale and convective structure of a hurricane rainband. *J. Atmos. Sci.,* **40,** 2125-2137.

Bryan, G., R. Rotunno and Y. Chen, 2009: *The effects of turbulence on hurricane intensity*. 29th Conference on Hurricanes and Tropical Meteorology.

Chan, J. C., and J.D. Kepert, 2010: *Global perspectives on tropical cyclones: From science to mitigation, 2nd edition*. World Scientific.

Chen, S. and J. Dudhia, 2000: *Annual Report: WRF Physics*. URL: http://www2.mmm.ucar.edu/wrf/users/docs/wrf-doc-physics.pdf

Chen, Y. and Kurkutes, S., 2012: *Impacts of turbulence length scales on numerical forecasts of Hurricane Earl (2010).* American Meteorological Society. URL: https://ams.confex.com/ams/30Hurricane/webprogram/Paper206082.html.

Eliassen, A., 1951: Slow thermally or frictionally controlled meridional circulation in a circular vortex. *Astrophysica Norvegica,* **2,** 18-60. URL: http://adsabs.harvard.edu/full/1951ApNr....5...19E.

Fortner, L. E., 1958: Typhoon Sarah, 1956. *Bull. Amer. Meteo. Soc.,* **30,** 633-639.

Hawkins, H. F., 1983: Hurricane Allen and island obstacles. *J. Atmos. Sci,* **40,** 1360-1361.

Hawkins, H. F., and D. T. Rubsam, 1968: Hurricane Hilda, 1964. *Mon. Wea. Rev.,* **96,** 701-707.

Hence, D., and R. A. Houze, 2008: Kinematic structures of convective-scale elements in the rainbands of Hurricane Katrina and Rita (2005). *J. Atmos. Sci.,* **113,** D15108, doi:10.1029/2007JD009429.

Houze, R. A., S. S. Chen, W. Lee, R. F. Rogers, J. A. Moore, G. J. Stossmeister, M. M. Bell, J. Cetrone, W. Zhao, and R. Brodzik, 2005: The hurricane rainband and intensity change experiment: Observations of modelling Hurricanes Katrina, Ophelia, and Rita. *Amer. Meteo. Soc.,* BAMS, 1503-1521.

Houze, R. A., Chen, S., Smull, B., Lee, W., and Bell, M, 2007: Hurricane intensity and eyewall replacement. *Science Magazine.,* **315,** 1235-1240.

Huang, Y. -H., M.T. Montgomery and C.-C. Wu, 2012: Concentric eyewall formation in Typhoon Sinlaku (2008). Part II: Axisymmetric dynamical processes. *J. Atmos. Sci.,* **69,** 662-674.

Judt, F., and S. S. Chen, 2010: Convectively generated potential vorticity in rainbands and formation of the secondary eyewall in Hurricane Rita of 2005. *J. Atmos. Sci.,* **67,** 3581-3599.

Kain, J. S., and J. M. Fritsch, 1990: Convective parameterization for mesoscale models: The Kain-Fritsch scheme. The representation of cumulus convection in numerical models*, Meteo. Monogr.,* No. 46, 165-170.

Kepert, J. D., 2013: How does the boundary layer contribute to eyewall replacement cycles in axisymmetric tropical cyclones? *J. Atmos. Sci.,* **70,** 2808-2830.

Kimberlain, Todd B., 2010: *Tropical cyclone report Hurricane Danielle*. National Hurricane Center. URL: http://www.nhc.noaa.gov/data/tcr/AL062010_Danielle.pdf.

Knabb, Richard D., Daniel P. Brown, and Jamie R. Rhome, 2006: *Tropical cyclone report Hurricane Rita*. National Hurricane Center. URL: http://www.nhc.noaa.gov/data/tcr/AL182005_Rita.pdf.

Knowlton, C., 2013: Primary circulation. *The University of Rhode Island.* URL: http://www.hurricanescience.org/science/science/primarycirculation/.

Marks, F. D., 2003: *Hurricanes*. Ency. Atmos. Sci., Elsevier Science Limited, London, UK, 942-966.

Martinez, Y., G. Brunet, and M. K. Yau, 2010: On the dynamics of two-dimensional hurricane-like concentric rings vortex formation. *J. Atmos. Sci.,* **67,** 3253-3268.

Menelaou, K., M. K. Yau, and Y. Martinez, 2014: Some aspects of the problem of secondary eyewall formation in idealized three-dimensional nonlinear simulations. *J. Atmos. Sci.,* **6,** 491-512.

Meneveau, C., 2010: Turbulence: Subgrid-scale modelling. *Scholarpedia,* 5(1):9489.

Molinari, J., and D. Vollaro, 1990: External influences on hurricane intensity: Part II. Vertical structure and response of the hurricane vortex. *J. Atmos. Sci.,* **47,** 1902-1918.

Montgomery, M. T., and R. J. Kallenbach, 1997: A theory for vortex Rossby-waves and its application to spiral bands and intensity changes in hurricanes. *Quart. J. Roy. Meteo. Soc.,* **123,** 435-465.

Moon, Y., and D. S. Nolan, 2010: The dynamic response of the hurricane wind field to spiral rain band heating. *J. Atmos. Sci.,* **67,** 1779-1805.

Nong, S., and K. A. Emanuel, 2003: A numerical study of the genesis of concentric eyewalls in hurricanes. *Quart. J. Roy. Meteo. Soc.,* **129,** 3323-3338.

Ortt, D., 2007: Effects of environmental water vapor on tropical cyclone structure and intensity. University of Miami, Scholarly Repository. MSc. Thesis.

Peng, J., M. S. Peng, and T. Li, 2008: Dependence of vortex axisymmetrization on the characteristics of the asymmetry. *Quart. J. Roy. Meteo. Soc.,* **134,** 1253-1268.

Pidwirny, M., 2012: *Tropical weather and hurricanes*. The Encyclopedia of Earth. URL: http://www.eoearth.org/view/article/156717/.

Qiu, X., Z.-M. Tan, and Q.-N. Xiao, 2010: The roles of vortex Rossby waves in hurricane secondary eyewall formation. *Mon. Wea. Rev.,* **138,** 2092-2109.

Rotunno, R., G. Bryan, and Y. Chen, 2012: *Impacts of turbulence on hurricane intensity*. URL: http://www.nopp.org/wp-content/uploads/project-reports-cdrom/reports/12YChen.pdf

Rozoff, C. M., W. H. Schubert, D. Brian, and J. Kossin, 2006: Rapid filamentation zones in intense tropical cyclones. *J. Atmos. Sci.,* **44,** 542-561.

Rozoff, C. M., W. H. Schubert, and J. P. Kossin, 2008: Some dynamical aspects of tropical cyclone concentric eyewalls. *Quart. J. Roy. Meteo. Soc.,* **134,** 583-593.

Shapiro, L. J., and M. T. Montgomery, 1993: A three-dimensional balance theory for rapidly rotating vortices. *J. Atmos. Sci.,* **50,** 3322-3335.

Simpson, J., 2012: *Sandy no longer a hurricane*. Valley WX. URL: http://valleywx.com/2012/10/29/sandy-no-longer-a-hurricane/.

Skamarock, W. C., J. B. Klemp, J. Dudhia, D. O. Gill, B. M. Duda, X.-Y. Huang, W. Wei, and J. G. Powers, 2008: A description of the advanced research wrf version 3.0. *NCAR Technical Note*, **NCAR/TN-475+STR,** 1-113.

Smagorinsky, J., 1963: General circulation experiments with the primitive equations. *Mon. Wea. Rev.,* **93,** 99-164.

Smith, R. K. and M.T. Montgomery, 2016: The efficiency of diabatic heating and tropical cyclone intensification. *Q. J. R. Meteorol. Soc.*, **00**, 1-7.

*S*tewart, Stacy R., 2004: T*ropical cyclone report Hurricane Ivan*. National Hurricane Center. URL: http://www.nhc.noaa.gov/data/tcr/AL092004_Ivan.pdf.

Sun, Y. Q., Y. Jiang, B. Tan, and F. Zhang, 2013: The governing dynamics of the secondary eyewall formation of Typhoon Sinlaku (2008). *J. Atmos. Sci.,* **70,** 3818-3837.

Terwey, W. D., and M. T. Montgomery, 2008: Secondary eyewall formation in two idealized, full-physics modeled hurricanes. *J. Geophys. Res.,* **113,** D12112, doi: 10.1029/2007JD008897.

Thornton, M. A., 2006: *Hurricane structure*. Lake Erie WX. URL: http://www.lakeeriewx.com/Meteo241/ResearchTopicFour/Hurricane Structure.html.

Wang, Y., 2002: Vortex Rossby waves in a numerically simulated tropical cyclone. Part II: The role in tropical cyclone structure and intensity changes. *J. Atmos. Sci.,* **59,** 1239-1262.

Wang, Y., 2009: How do outer spiral rainbands affect tropical cyclone structure and intensity? *J. Atmos. Sci.,* **66,** 1250-1273.

Wang, X., Y. Ma, and N. E. Davidson, 2013: Secondary eyewall formation and eyewall replacement cycles in a simulated hurricane: Effect of the net radial force in the hurricane boundary layer. *J. Atmos. Sci.,* **70,** 1317-1341.

Willoughy, H. E., 1979: Forced secondary circulations in hurricanes. *J. Geophys. Res.,* **84,** 3173-3183.

Willoughby, H. E., J. A. Clos, and M. G. Shoreibad, 1982: Concentric eyewalls, secondary wind maxima, and the evolution of the hurricane vortex. *J. Atmos. Sci.,* **39,** 395-411/

Wu, L., and S. A. Braun, 2003: Effects of convective asymmetries on hurricane intensity: A numerical study. *J. Atmos. Sci.,* **61,** 3065-3081.

Yano, Jun-Ichi, and Kerry Emanuel, 1991: An Improved Model of the Equatorial Troposphere and Its Coupling with the Stratosphere. *Journal of the Atmospheric Sciences*, **48**, 377-389.

Zhang, J. A., 2010: Spectral characteristics of turbulence in the hurricane boundary layer over the ocean between the outer rain bands. *Quart. J. Roy. Meteor. Soc.*, **136**, 918-926.

Zhang, J. A., and M. T. Montgomery, 2012: Observational estimates of the horizontal eddy diffusivity and mixing length in the low-level region of intense hurricanes. *J. Atmos. Sci.,* **69,** 1306-1316.

Zhou, X., and B. Wang, 2011: Mechanisms of concentric eyewall replacement cycles and associated intensity change. *J. Atmos. Sci.,* **68,** 972-988.

Zhu, Z., 2014: *Mechanisms governing the eyewall replacement cycle in numerical simulations of tropical cyclones*. Florida International University, FIU Digital Commons. Ph.D. Thesis.

Zhu, Z., and P. Zhu, 2015a: The role of outer rainband convection in governing the eyewall replacement cycle in numerical simulations of tropical cyclones. *J. Atmos. Sci.,* **119,** 8049-8072.

Zhu, Z. and P. Zhu, 2015b: Sensitivities of eyewall replacement cycle to model physics, vortex structure, and background winds in numerical simulations of tropical cyclones. *J. Atmos. Sci.,* **120,** 590-622.